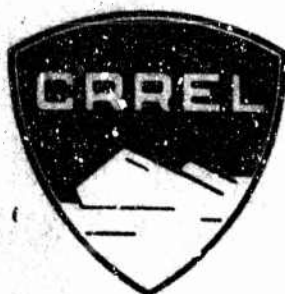


TR 190



AD 680902

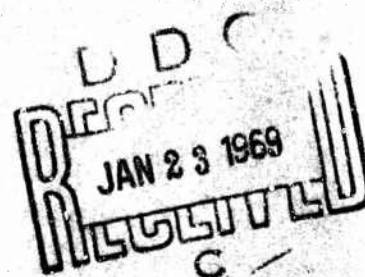
Technical Report 190

CREEP OF FROZEN SANDS

by

Francis H. Sayles

September 1968



CONDUCTED FOR
CORPS OF ENGINEERS, U.S. ARMY

BY

U.S. ARMY MATERIEL COMMAND
TERRESTRIAL SCIENCES CENTER

COLD REGIONS RESEARCH & ENGINEERING LABORATORY
HANOVER, NEW HAMPSHIRE

THIS DOCUMENT HAS BEEN APPROVED FOR PUBLIC RELEASE
AND SALE; ITS DISTRIBUTION IS UNLIMITED.

Report prepared by the
CLEARINGHOUSE
for Federal Laboratories
Information and Proprietary

63



Technical Report 190

CREEP OF FROZEN SANDS
by
Francis H. Sayles

September 1968

CONDUCTED FOR
CORPS OF ENGINEERS, U.S. ARMY
BY
U.S. ARMY MATERIEL COMMAND
TERRESTRIAL SCIENCES CENTER
COLD REGIONS RESEARCH & ENGINEERING LABORATORY
HANOVER, NEW HAMPSHIRE

THIS DOCUMENT HAS BEEN APPROVED FOR PUBLIC RELEASE
AND SALE; ITS DISTRIBUTION IS UNLIMITED.

PREFACE

Authority for the investigation reported herein is contained in FY 1961 Instructions and Outline, Military Construction Investigations, Engineering Criteria and Investigations and Studies, Investigation of Arctic Construction, Creep of Frozen Soils.

This study was conducted for the Engineering Division, Directorate of Military Construction, Office, Chief of Engineers. The program was administered by the Civil Engineering Branch, Mr. T.B. Pringle, Chief.

Mr. Francis H. Sayles, Research Civil Engineer, Applied Research Branch carried out the study and prepared this report. The investigation was under the general direction of Mr. K.A. Linell, Chief, Experimental Engineering Division, and the immediate direction of Mr. Albert F. Wuori, Chief, Applied Research Branch, Cold Regions Research and Engineering Laboratory (CRREL), U.S. Army Terrestrial Sciences Center (USA TSC). Personnel assisting in the investigation were SP Richard Putnam and SP Richard O. Lunde. Mr. Robert Bonnett assisted in the testing.

This report has been critically reviewed by Professor Clyde E. Kesler of the University of Illinois and by Mr. Frederick J. Sanger of USA TSC. The author wishes to thank the reviewers and Dr. A. Assur, Chief Scientist, USA TSC, for their constructive suggestions.

Lieutenant Colonel John E. Wagner was Commanding Officer/Director of the U.S. Army Terrestrial Sciences Center during the publication of this report and Mr. W.K. Boyd was Chief Engineer.

USA TSC is a research activity of the Army Materiel Command.

CITATION OF COMMERCIAL PRODUCTS IS FOR INFORMATION ONLY
AND DOES NOT CONSTITUTE OFFICIAL ENDORSEMENT OR APPROVAL.

CONTENTS

	Page
Preface -----	ii
Conversion table -----	v
Summary -----	vi
Introduction -----	1
Definition of terms-----	1
Review of theory-----	2
Testing-----	4
Apparatus-----	5
Materials-----	11
Preparation and freezing of test specimens-----	12
Creep and strength testing procedure -----	14
Test results-----	14
Discussion-----	23
Conclusions-----	46
Literature cited -----	47
Appendix A.-----	49

ILLUSTRATIONS

Figure

1. Mechanical rheological models-----	3
2. View of four freezing cabinets inside 40F cold room-----	5
3. Front of freezing cabinet-----	6
4. Freezing mold -----	7
5. Freezing mold charged with specimens being de-aired and saturated -----	8
6. Pneumatically actuated hydraulic press -----	8
7. Constant stress apparatus-----	9
8. Lever-type press with motorized moving fulcrum-----	10
9. Unconfined compression chamber -----	10
10. Gradation curve, Manchester fine sand -----	12
11. Typical Ottawa sand specimens after testing-----	15
12. Typical Manchester fine sand specimens after testing -----	16
13. Typical ice specimens after testing-----	17
14. Creep tests, Ottawa sand (20-30), 15F-----	18
15. Creep tests, Manchester fine sand, 15F -----	18
16. Creep test on ice in unconfined compression-----	19
17. Time vs strain, Ottawa sand (20-30), 15F-----	19
18. Time vs strain, Ottawa sand (20-30), 25F-----	20
19. Time vs strain, Ottawa sand (20-30), 29F-----	20
20. Time vs strain, Ottawa sand (20-30), 31F-----	21
21. Time vs strain, Manchester fine sand, 15F -----	21
22. Time vs strain, Manchester fine sand, 25F -----	22
23. Time vs strain, Manchester fine sand, 29F -----	22
24. Time vs strain, Manchester fine sand, 31F -----	23
25. Rebound and classical creep curves, Ottawa sand-----	24
26. Percent of strain at start of tertiary creep, Manchester fine sand -----	28
27. Creep rate and time, Ottawa sand (20-30), 31F -----	28
28. Creep rate and reciprocal of time, Ottawa sand, 31F-----	29
29. Creep rate and reciprocal of time, Manchester fine sand, 15F -----	29

CONTENTS (Cont'd)

Figure		Page
30.	Creep rate and reciprocal of time, Manchester fine sand at various temperatures-----	30
31.	Stress, strain and time, 31F -----	32
32.	Time, factor A, and temperature -----	32
33.	Factor R and temperature-----	33
34.	Strain and time - comparative curves, 15F -----	34
35.	Factor M and stress -----	34
36.	Strain and time, 15F -----	35
37.	Strain rate at time 1 hr, and stress -----	36
38.	Temperature and stress for unit strain rate at 1 hr -----	36
39.	Ultimate strength and time to failure, Ottawa sand -----	39
40.	Ultimate strength and time to failure, Manchester fine sand -	39
41.	Time and reciprocal of ultimate stress, Manchester fine sand	41
42.	Time and reciprocal of ultimate stress, Ottawa sand -----	41
43.	Strength for various conditions, Ottawa sand-----	43
44.	Strength for various conditions, Manchester fine sand-----	43
45.	Temperature, β and B parameters -----	44

TABLES

Table

I.	Types of deformations from rebounded creep tests, frozen Ottawa sand-----	25
II.	Strain components and strain at critical points under inter- mediate stresses-----	26
III.	Value of m in Vialov's strain equation-----	31
IV.	Constants for Vialov's strain equation-----	31
V.	Constants for strain equation -----	37
VI.	Long-term unconfined compressive strength-----	40
VII.	Constants for eq 7 as determined from Figures 41 and 42 ---	40
VIII.	Percent of instantaneous strength loss after application of stress-----	42

CONVERSION TABLE

<u>Multiply</u>	<u>By</u>	<u>To obtain</u>
°F	$5/9(°F - 32)$	°C or °K
in.	25.4	mm
ft	30.48	cm
sq in.	6.4516	sq cm
lb/sq in.	0.070307	kg/sq cm
cu ft	0.0283168	cu m
lb	0.45359237	kg
qt	0.94633	liter

SUMMARY

Unconfined compressive creep strengths and strains were measured for frozen saturated Ottawa sand (20-30) and Manchester fine sand. The creep tests were conducted at approximate stress levels of 60, 35, 20 and 5% of the conventional unconfined compressive strength. Testing temperatures were 15, 25, 29 and 31F. It was found that the unconfined compressive creep strength of the frozen sand can be predicted using Vialov's strength formula; that creep strain can be predicted using two short-term, high-stress-level creep tests using $\epsilon = \epsilon_1 \cdot \frac{t^\psi}{\psi}$; that total strain can be predicted using $\epsilon = \left[\frac{\sigma}{\sigma_{01} \theta_0^a [\theta/\theta_0] + 1} \right]^{1/K} \frac{t^\psi}{\psi} + \epsilon_0$; and that for stresses below the long-term strength, the strain rate is directly proportional to the reciprocal of time during stress action until complete stabilization occurs. (ϵ_1 = strain rate 1 hour after stress is applied; t = time; $\psi = (M-1)/M$, where $M = \sigma^1/w$ and w is a constant for each material; σ_{01} = stress at $\theta = 0$; θ = temperature in degrees below freezing point of water; θ_0 = a constant reference value of θ ; a and K are constants; ϵ_0 = initial instantaneous strain.)

CREEP OF FROZEN SANDS

by

Francis H. Sayles

INTRODUCTION

The design of stable structures on permafrost requires a knowledge of the strength and deformation characteristics of frozen soil. Published material on the strength and deformation properties of frozen soil prior to 1952 was of Russian origin and was generally incomplete as to description of soils and testing procedures. In 1952 the former Arctic Construction and Frost Effects Laboratory (ACFEL)* of the U. S. Army Engineer Division, New England, published a report summarizing experimental data obtained up to that time, including the results of their investigations (ACFEL, 1952). Since 1952 the Russians, notably Tsytovich and Vialov, have published rather complete experimental data on the strength and deformation properties of some naturally frozen silts and clays (Tsytovich, 1954, 1958; Vialov, 1959; Vialov et al., 1962; Vialov and Tsytovich, 1955). In addition, they summarized and formulated theories and empirical equations relating strength and deformation of frozen soils to the soil temperature and duration of the applied load. Sanger and Kaplar (1963) published deformation data and empirical equations relating unconfined compressive deformation and rate of deformation to applied stress and temperature. This investigation included a variety of soils, tested at various temperatures from about 18F to 32F. Each creep test was limited to 60 hours duration.

The purpose of this investigation is to evaluate the influence of temperature and stress on creep and long-term strength of saturated frozen sands, and to provide data for design in frozen soils.

This report with its appendix presents the completed results of the unconfined compression tests performed on saturated Ottawa sand (20-30) and Manchester fine sand. This is only the first phase of the current investigation which includes: (1) unconfined compression creep tests on Ottawa sand, Manchester fine sand, New Hampshire silt and a clay and (2) triaxial creep testing of Ottawa sand.

DEFINITION OF TERMS

Instantaneous strength is the maximum stress determined by loading the test specimen at a constant strain rate of 0.033/min.

Long-term strength is the maximum stress that the frozen soil can withstand indefinitely and exhibit either a zero or continuously decreasing strain rate with time.

* ACFEL was merged with the former U.S. Army Snow, Ice and Permafrost Research Establishment (SIPRE) in 1961 to form the U.S. Army Cold Regions Research and Engineering Laboratory.

CREEP OF FROZEN SANDS

Conventional strain is the axial deformation divided by the original length of the specimen ($e_c = \Delta L / L_0$).

True strain is the axial deformation at a given instant of time divided by the actual specimen length at that time [in terms of conventional strain, $e_t = \ln(1/(1-e_c))$].

Incipient failure of a test specimen occurs when the strain rate starts to increase with time (start of tertiary creep), after a period of minimum strain rate (point i, Fig. 25).

Failure of a compression test specimen of frozen sand means a continuous loss of resistance to loading, after reaching a peak. It occurs by either an abrupt brittle-type fracture or a plastic flow accompanied by fissuring and often ending in rupture of the specimen.

Elastic deformation disappears entirely upon release of the stress which caused it.

Delayed elastic deformation is elastic deformation that requires a noticeable period of time to occur or recover. Theoretically, elastic deformation velocities slower than the speed of sound are delayed. In this report delayed elastic recovery is slower than the speed of sound periods by hours and days.

Viscous deformation is an irreversible deformation in which the rate of deformation depends upon the applied stress.

Plastic deformation is an irreversible deformation which is independent of time.

Stress ratio, $\rho = \frac{\text{Applied constant stress}}{\text{"instantaneous" strength}}$.

REVIEW OF THEORY

Deformation

Vialov and Tsytovich (1955) explain the physical process of creep in frozen soil by considering the condition of applying a constant load to a frozen soil mass. This load concentrates the stress between the soil particles at their points of contact with the ice, causing pressure-melting of the ice. Differences in water surface tensions are produced and the unfrozen water moves to regions of lower stress where it refreezes. The process of ice melting and water movement is accompanied by a breakdown of the ice and structural bonds of the soil grains, the plastic deformation of the pore ice and a readjustment in the particle arrangement, the result of which is the time-dependent deformation phenomenon of creep. This structural deformation leads to a denser packing of the soil particles, which in turn causes a strengthening of the material due to the increased number of firm contacts between soil grains and hence an increase in internal friction between grains (ACFEL, 1952). During this process there is also a weakening of the structural cohesion and possibly an increase in the amount of unfrozen water in the frozen soil (particularly in fine-grained soils). All of this action is time-dependent. If the applied load does not exceed the long-term strength of the frozen soil, then the weakening process is compensated by the strengthening; the deformation is damped, i.e., the rate of deformation decreases with time. However, if the applied load exceeds the frozen soil long-term strength, the breakdown of internal bonds is not completely compensated by the strengthening process and then the rate of

CREEP OF FROZEN SANDS

3

deformation increases with time, resulting in undamped deformation which eventually develops into plastic flow and ends in a breakdown of the frozen soil structure.

Experiments* show that the deformation characteristics of frozen soil are similar to those depicted by the classical creep curve for metals (Fig. 1). As an aid in studying these deformation characteristics, Vialov and others have proposed mechanical rheological models. In Figure 1, Vialov's model (1959) with the various components labeled, depicts the first and second stages of creep, but does not include the initial plastic deformation or third stage of creep, i.e., the visco-plastic flow preceding complete collapse of the material structure.

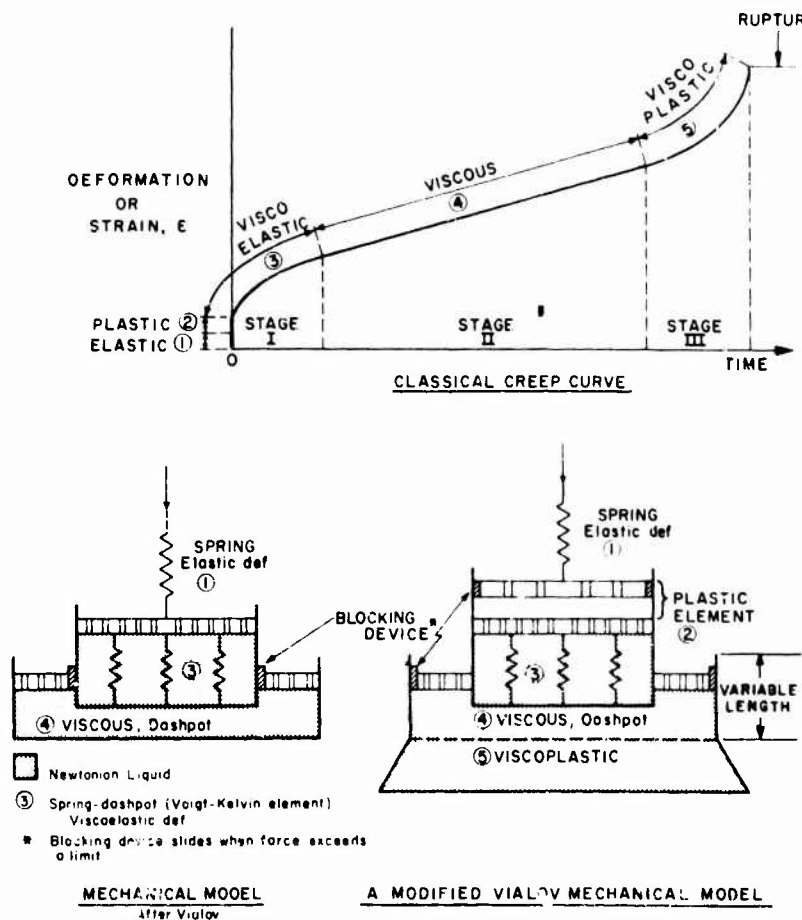


Figure 1. Mechanical rheological models.

* Vialov, 1962, Fig. 27, (Translation page 101) for silt and clay and Figures 14 and 15 of this report for saturated Ottawa sand and Manchester fine sand.

CREEP OF FROZEN SANDS

In Figure 1 Vialov's model is modified to include plastic characteristics. The various elements on the model are labeled to correspond to the appropriate section of the classical creep curve. In the modified model, the initial plastic deformation is represented by a frictional slide. An air gap (this gap may have finite value or be zero) between the slide and the Voigt element permits displacement to take place before viscoelastic movement begins. If the load exceeds the yield point of the material, the slide will move to reduce or close the gap, thus producing instantaneous plastic deformation. When the load is removed, this part of the deformation is not recovered. In some instances elastic deformation may occur without reaching the plastic limit upon loading, thus producing purely elastic deformation. The viscoelastic element is the Voigt or Kelvin element which contributes a delayed elastic effect. The dashpot of element 4 represents the viscous portion of the curve. The friction element (blocking device) requires the activating force to reach a certain magnitude before plastic and viscous deformation can occur. To represent viscoplastic flow a specially shaped dashpot is shown to permit an increasing rate of flow as the material approaches failure. The modified model is too complicated for a practical numerical analysis and is merely shown to illustrate the deformation components.

Strength.

Strength of frozen soils, as with unfrozen cohesive soils, depends upon both the cohesion and the internal friction of the component materials. In frozen soils the cohesion component according to Vialov and Tsytovich (1955) can be attributed to: (1) the molecular forces of attraction between solid particles; (2) physical or chemical cementing of particles together; and (3) cementing the soil particle by ice formation in the soil voids. Cementing by ice is the result of the bonds between the ice crystals and the soil particles even though the soil particles are surrounded by a film of unfrozen water. This unfrozen water is under the influence of molecular forces of the soil particles and it seems possible that the strongly attached water molecules are capable of transmitting normal and shear forces between solid ice and solid grains. The ice cohesion depends upon the amount of ice, the strength of the ice, and the area of ice in contact with the soil particles, each of which depends upon the soil temperature. The internal friction depends on the soil grain arrangement, sizes, distribution, shape, and on the number of grain-to-grain contacts. It is emphasized that ice cohesion is the dominant strength factor in frozen soil even though internal friction becomes significant in dense sands.

TESTING

Types

The unconfined compression test was chosen as the primary test for this investigation because of its simplicity and its suitability for adoption as a field laboratory test.

In addition to the compression test, sonic tests and ball penetration tests were performed. The sonic tests were exploratory in nature with the primary purpose of testing equipment and developing techniques. Both tests showed some promise but the allotted time did not permit continuance until techniques could be perfected.

APPARATUS

Freezing facilities

Soil and ice specimens were frozen in freezing cabinets mounted in a USA CRREL walk-in type cold room maintained at $+40F \pm 1F$. The freezing cabinets used in this project (Fig. 2, 3) were equipped with hinged covers on top and a thermal-pane window in the front. Insulation was provided in the sides and cover. The bottom of the cabinet consisted of an expanded metal grill allowing the bottom of the specimens to be exposed to the $40F$ room temperature during freezing while the tops of the specimens were subjected to the desired freezing temperature. The freezing cabinet was cooled by coils mounted in its sides and back wall, from 13 in. above the bottom to the top of the cabinets.

The cabinet temperature could be controlled to within $\pm 0.5F$ by means of heating coils located in the air stream of the air circulation fan. The heat supplied was regulated by a Bayley temperature controller Model 122. De-aired water was supplied to the bottom of the specimens during freezing by means of an external reservoir.

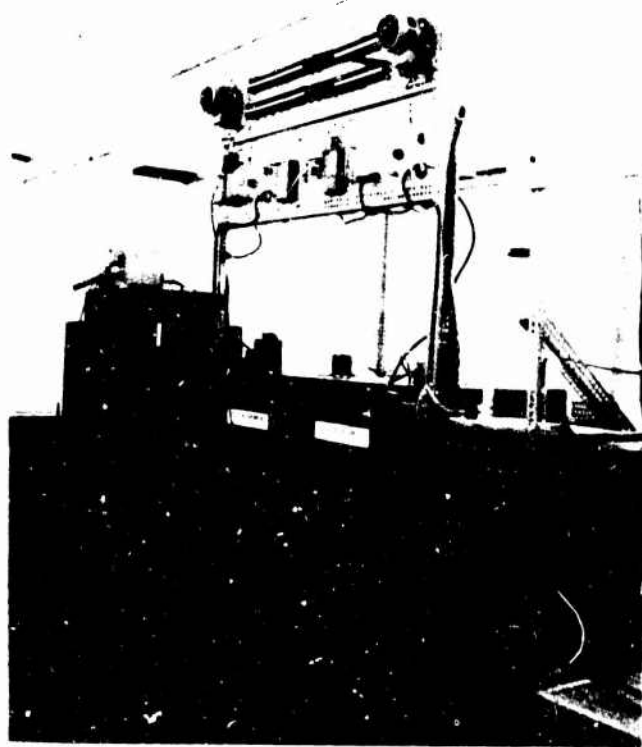


Figure 2. View of four freezing cabinets inside $40F$ cold room.

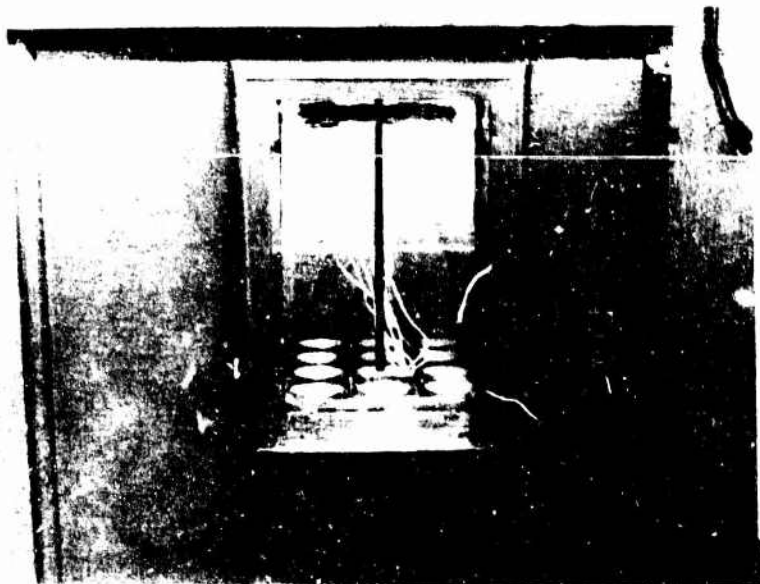


Figure 3. Front of freezing cabinet showing freezing mold in position with thermocouple leads to the center specimen. The bimetallic thermal-regulator is shown to right of viewing window.

Freezing mold

The freezing mold (Fig. 4, 5) consisted of a Plexiglas block 17 1/4 in. square and 7 in. thick, through which 25 3-in. diam holes were bored. Each hole was fitted with a split sleeve having a wall thickness of about 1/8 in. to permit specimen ejection from the mold without subjecting the specimen to the ejection force. The top and bottom of the mold were covered by 1/2-in. thick aluminum plates sealed to the mold block with 1/2-in. soft rubber gaskets. When the freezing mold was assembled, an expanded metal screen with 1/2 x 1/4-in. openings, a 200-mesh bronze screen and a muslin mat were placed at the top and bottom of the mold block to retain the unfrozen soil specimens in the cylinders and to act as a filter.

Loading equipment

Three types of loading devices were used in the testing program to accommodate the different strength and deformation characteristics of the frozen sands.

Tests to determine the instantaneous compressive strength and short-term creep strength of frozen soils with relatively high resistance were performed in a 20,000-lb capacity air-actuated hydraulic press (Fig. 6). Loads were applied to the test specimen by means of an unconfined test chamber placed in the press. The press is capable of head movement rates up to 18 in./min. For creep tests, vibration-free constant loads can be maintained by the hydraulic press for extended periods of time within 2% of the applied load for loads greater than 3000 lb.

CREEP OF FROZEN SANDS

7

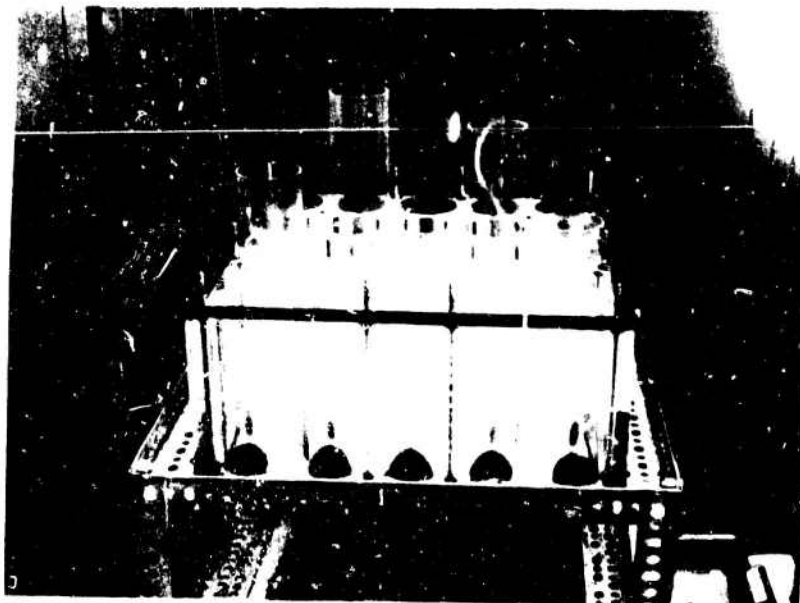


Figure 4a. Empty freezing mold showing projecting split sleeves.

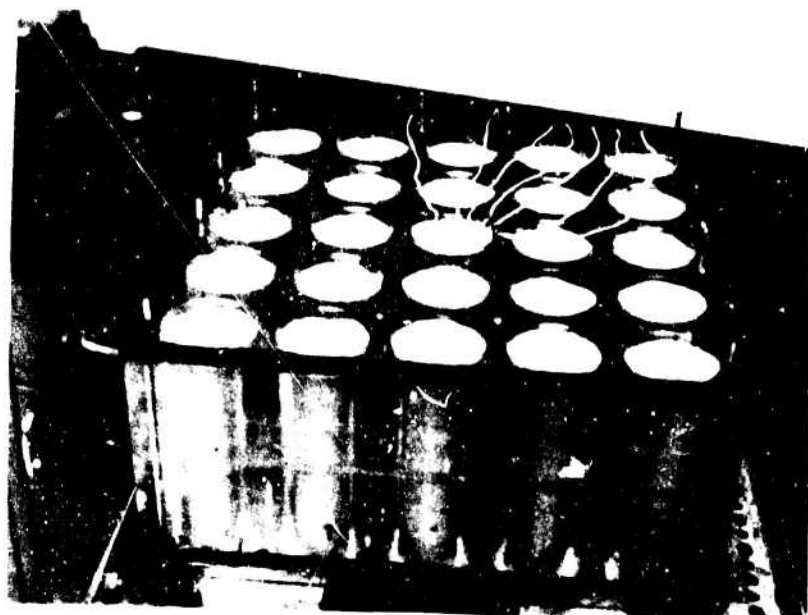


Figure 4b. Freezing mold filled with dry sand showing split sleeves. Mold is supported on ejection frame.

CREEP OF FROZEN SANDS

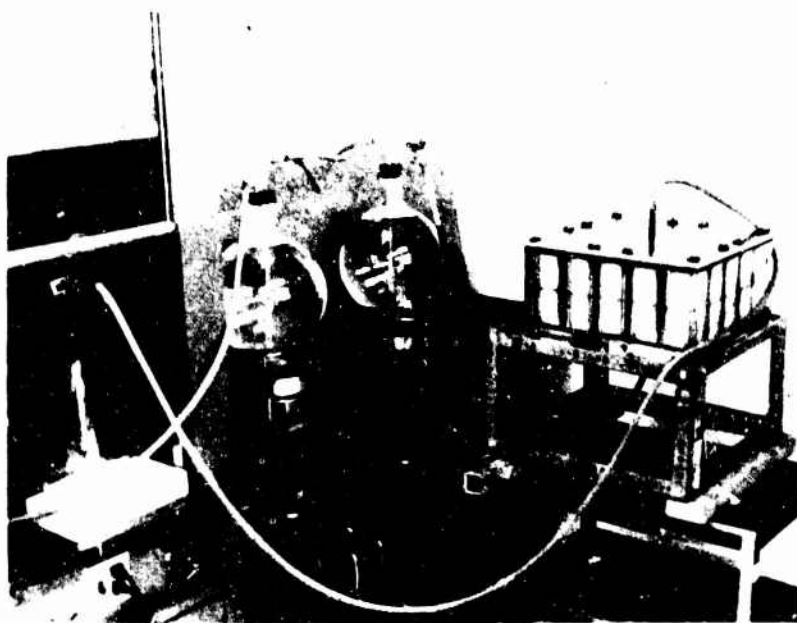


Figure 5. Freezing mold charged with specimens being de-aired and saturated.



Figure 6. Pneumatically actuated hydraulic press.



Figure 7. Constant stress apparatus showing programming cam and load measuring system.

ured by two linear motion potentiometers mounted diametrically opposite each other on the circumference of the load transducer.

Load and deformation measurements

All loads applied to test specimens in the hydraulic and constant stress presses were measured with Baldwin-Lima-Hamilton load cells having appropriate load ranges.

Hydraulic press loads were measured using the load cells with readout on one channel of a Leeds and Northrup Azar G-type X-X recorder. After calibration, loads were measured continuously to within 1.0% of the applied load.

Average axial deformations of test specimens in the hydraulic press were measured using two carbon-strip, infinite-resolution, resistance-type linear-motion potentiometers mounted diametrically opposite each other on the load cell (see Fig. 9), and movements were recorded on one channel of the L and N recorder. Using calibration charts, deformations were measured to within 0.0025 in. for movements less than 0.25 in. and 0.005 in. for movements greater than 0.25 in.

Creep tests in which large deformation occurs were performed on a constant stress press (capacity 4000 lb) (Fig. 7). This press features a programming cam that maintains constant axial stress to within 1% of applied stress on the test specimen during deformation. The load-programming is based on the assumptions that the cross-sectional area of the specimen remains uniform throughout its length during deformation, and that the volume remains constant throughout the test.

Long-term creep tests resulting in small deformation were performed on a lever-type press (capacity 2000 lb) (Fig. 8). As the sample deforms, the height of the fulcrum is adjusted to maintain the loading level approximately horizontal.

Test chamber

The unconfined compression chamber in the hydraulic press (Fig. 9) is basically a frame with a leveling base upon which the test specimen rests. The loading piston mounted in recirculating ball bushings provides a base plate for the load measuring transducer. This transducer is in direct contact with the top spherical surface of the test specimen end cap. This arrangement permits measurement of the load applied to the test specimen at any time. Average deformations are mea-

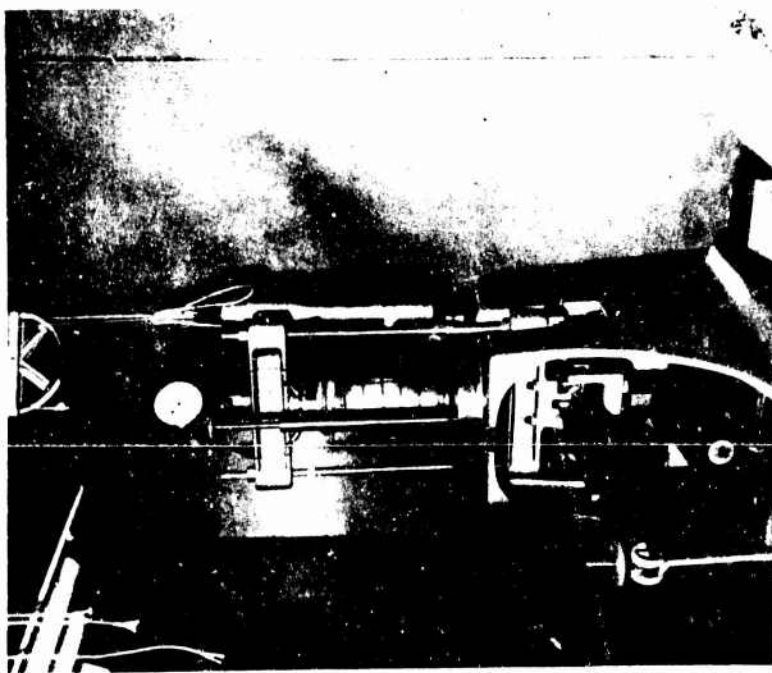


Figure 8. Lever-type press with motorized moving fulcrum.

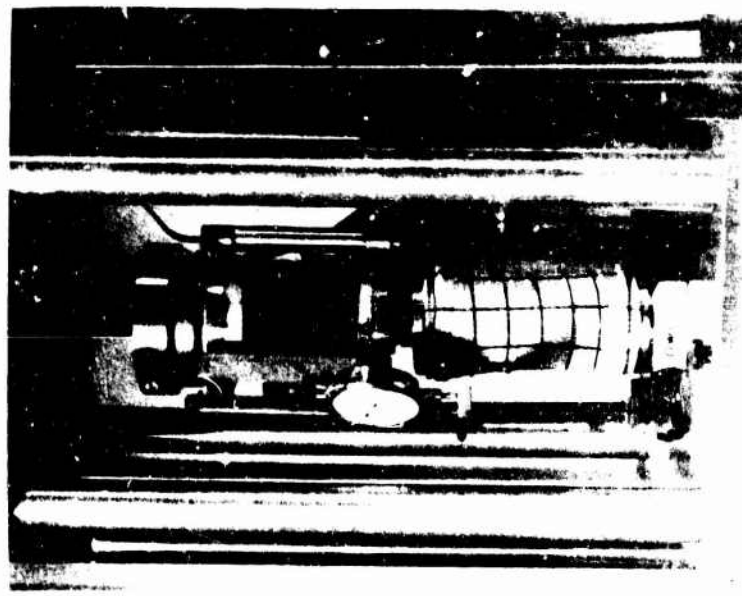


Figure 9. Unconfined compression chamber showing load and deformation transducers.

Constant-stress-apparatus loads were measured with the load cell and read manually using a B-L-H type N portable strain indicator. Loads were determined accurately to within 0.3% of the applied load. Deformations were measured using dial indicators with 1/10,000 in. gradations and a sensitivity of 2/100,000 in. (See Figure 7 for arrangement of load cell and dial indicators.)

Constant load lever-type-press loads were determined by computing the hanger weights using the lever arm ratio. The load applied to each specimen was checked by placing a load cell in the specimen test space and reading the load with the hanger weights in place. Deformations were measured using the same type of extensometer as was used in the constant stress apparatus (see Fig. 7).

Temperature control

Test temperatures of 25F and lower in the walk-in cold room were controlled to within $\pm 1^{\circ}\text{F}$. To damp temperature fluctuations to less than $\pm 0.50^{\circ}\text{F}$, tests were conducted in inclosures constructed of 2 in. thick rigid type insulation (Styrofoam).

Test temperatures above 25F were controlled by heating and circulating air within the insulated test inclosures. Each test specimen was housed in a split Lucite cylinder to reduce temperature fluctuations of the air surrounding it. Heat was supplied by light bulbs mounted in the fan air-stream. The temperature was regulated by a mercury-column-type thermoregulator which activated a relay to supply heat upon demand.

Air temperatures within the Lucite inclosures surrounding the test specimen were held constant well within $\pm 0.1^{\circ}\text{F}$ of the desired temperature.

Temperature measurements

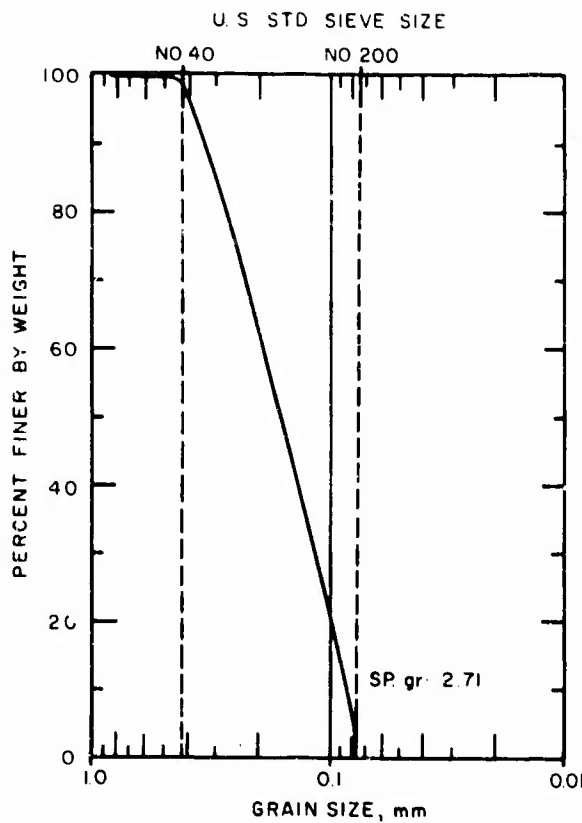
Temperatures 25F and lower were measured to the nearest 0.5°F with a mercury thermometer placed within the insulated inclosures. Inside the Lucite inclosure a thermistor sensed the temperature of the air surrounding the test specimen and the readings were recorded every 1.25 min on a 12-point L and N type H recorder, to the nearest 0.2°F . Test temperatures above 25F were measured to within 0.1°F using the same sensing and recording system but with increased sensitivity. Thermistor readings were checked daily using a manually operated Wheatstone bridge. Cold-room temperatures (outside of inclosures) were recorded continuously.

MATERIALS

Ottawa sand (20-30) and Manchester fine sand were tested. Ottawa sand represents a nearly idealized granular soil. Manchester fine sand is a natural sand with quite uniform gradation; it is finer than Ottawa sand (see Fig. 10 for gradation).

A limited number of ice specimens frozen under the same conditions as those for the soils were tested as a correlation material and to obtain ice-test data using the same testing equipment. Ice-specimen densities were less than that for solid ice because of air entrapment during freezing. (See Table AIII, App. A, for densities.)

CREEP OF FROZEN SANDS



SAND		SILT OR CLAY
Med.	Fine	

Figure 10. Gradation curve, Manchester fine sand.

PREPARATION AND FREEZING OF TEST SPECIMENS

Specimen molding

The soil specimens were molded, saturated and frozen in the Lucite mold previously described. To reduce friction during sample ejection from the mold, the outsides of the split sleeves were coated with silicone grease. The soil sample was not in direct contact with the grease. However, the split in the forming sleeve allowed saturating water to contact the silicone grease thus permitting only a slight chance of silicone contamination of the specimen. After the mold was assembled with the sleeves in position, the air-dry sands were placed in the mold in six equal layers, each tamped 10 times with a 1/4 in. diam steel rod (specimen densities are tabulated in Tables Ia, IIa, and IIIa). With top and bottom of the mold sealed, the soil-filled mold was evacuated to about 30 mm of mercury using a water ejection pump, and then the soil was saturated from the bottom by admitting de-aired water under vacuum into the bottom of the mold. After the mold was filled with water an additional 10 quarts of de-aired water percolated through the specimens to remove as much trapped air as possible. When saturation was completed the top and bottom mold connections were sealed for placement of the mold in the freezing cabinet.

Freezing

After saturation, the specimen-charged mold was placed in the freezing cabinet. Spaces between the sides of the mold and cabinet were insulated with granular cork. After removal of the top mold cover a de-aired water supply was connected to the bottom of the mold to permit specimen freezing in an open system. In this arrangement the bottoms of the specimens were exposed to 40F with a free water supply, and the tops were exposed to cold circulating freezing air. The rate of progress of the 32F isotherm was determined by means of thermocouples spaced 1 in. apart along the vertical axis of the center specimen. Soil samples were frozen within a period of 4 days, i.e., the average rate of frost penetration was 1 1/2 in. per day.

In freezing ice samples the procedure was similar to that outlined for soils. However, to reduce entrapment of air bubbles in the ice the rate of freezing was reduced to approximately 1/4 in. per day.

To remove the frozen specimens from the freezing mold, the mold was clamped in a specially constructed frame and each specimen was ejected by pressing against the split sleeve using a hydraulic jack with an ejector plate. The ejector plate diameter matched the mold bore and had a raised outer rim that permitted ejection of the specimen in the sleeve without loading the specimen. The split sleeve was removed from the ejected specimen by expanding its diameter with a thin blade inserted into the split.

Trimming

After removal of the split sleeve, the specimen was inspected for imperfections and cut to approximately a 6-in. height. Rough cutting was accomplished with a hacksaw and a wooden miter box. The ends were squared using a special case-hardened vee-shaped miter box and various gradations of wood rasps and steel files. After the specimen ends were trimmed to final length, the dimensions were determined by measuring the circumference (at the top, midheight, and bottom) and length (at six locations around the perimeter) to the nearest 1/1000 in. Variations in specimen length around the circumference were within ± 0.005 in. of the average except for about 10 specimens with variation up to ± 0.01 in. of the average. The diameter varied less than ± 0.003 in. along the specimen length.

The volume of each specimen was determined by submergence in liquid iso-octane (2, 2, 4 trimethylpentane) at 20F.

After volume determinations were made, Ottawa sand sample ends were capped with a thin layer of ice to avoid local stress concentrations at the relatively large sand grains in contact with the loading caps. The capping was accomplished by pouring a layer of 32F water on a flat glass plate, then setting the specimen end on the plate and allowing the water to freeze to the specimen in the cold room. The glass plate was removed by gently warming the outer surface of the plate.

It was not considered necessary to cap Manchester fine sand specimens with ice since the fine soil grains provided a smooth contact surface for the loading caps.

All specimens were sealed in circumferential rubber membranes and metal end caps for testing.

Storage and tempering

Prior to preparation for testing, the specimens usually remained in the sealed freezing mold. Occasionally it was necessary to eject several specimens

CREEP OF FROZEN SANDS

in advance of preparation for testing. These specimens were sealed in rubber membranes and temporary end caps, then sealed in plastic bags with crushed ice to eliminate sublimation. No change in specimen weight could be detected in weighings of selected specimens before and after storage. Storage periods did not exceed 6 weeks.

Before testing, all specimens were stored at the test temperature for a minimum of 48 hours. The required tempering time was checked using three thermocouples embedded at the midpoint and quarter points of the axial height of a control specimen. This check showed that 24 hours was sufficient time for the specimen to reach equilibrium at the test temperature.

CREEP AND STRENGTH TESTING PROCEDURE

At each test temperature a series of compression type tests was conducted by first determining the "instantaneous" strength* of the frozen soil or ice and then performing creep tests at reduced stress levels. Each test series included constant stress and constant load compression tests performed at stress levels of approximately 60, 35, 20, 10 and 2.5% (stress ratio, ρ) of the average instantaneous strength. One test series was conducted at each of the following test temperatures: 15, 25, 29 and 31°F. All compression type tests were performed on specimens 2.8 in. in diameter by 6 in. high. Whether constant-stress or constant-load tests were performed depended upon the magnitude of the applied stress and the expected deformation. Constant load tests were used for high stress and for small expected deformation at low stresses, while constant stress tests were performed at intermediate stress levels (i.e., in the range of $\rho = 15$ to 40%) where the deformations were expected to be large.

The compression creep test on each specimen was performed by first applying a seating load of approximately 2 psi to the specimen to insure positive contact between the test specimen and components of the loading system, and then applying the test load in less than 2 sec. Instantaneous strengths were determined by moving the loading press head against the specimen at a rate of 0.2 in. per min (strain rate of 0.033 per min). After each test was completed, photographs were taken of the test specimen (see Fig. 11 - 13 for typical specimens) and water contents were determined.

TEST RESULTS

Figures 14-16 show typical time-deformation curves (Ottawa sand, Manchester fine sand and polycrystalline ice) produced directly from data for each specimen subjected to the unconfined compression creep test. The time-strain curves on Figures 17 through 20 and Figures 21 through 24 summarize the data for Ottawa sand and Manchester fine sand respectively. (Where more than one specimen number is shown on a single curve, the curve represents the average of the curves obtained for specimens indicated and the vertical bars indicate the total range of values.) A summary of individual specimen data is shown in Appendix A.

* "Instantaneous" strength used herein is the maximum strength determined by loading the test specimen at a constant strain rate of 0.033 per min.

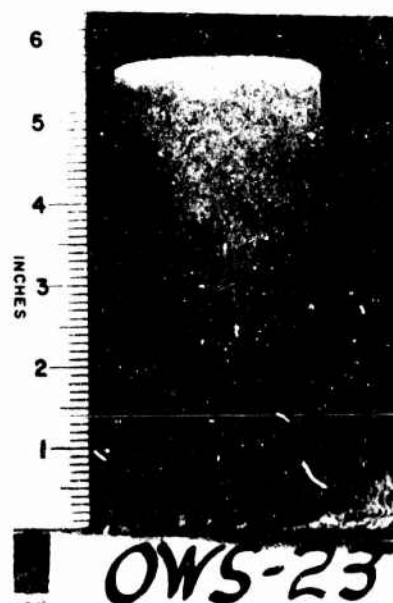


OWS-43

a. Brittle failure in instantaneous strength test. Temp, 25F, $e=0.58$.

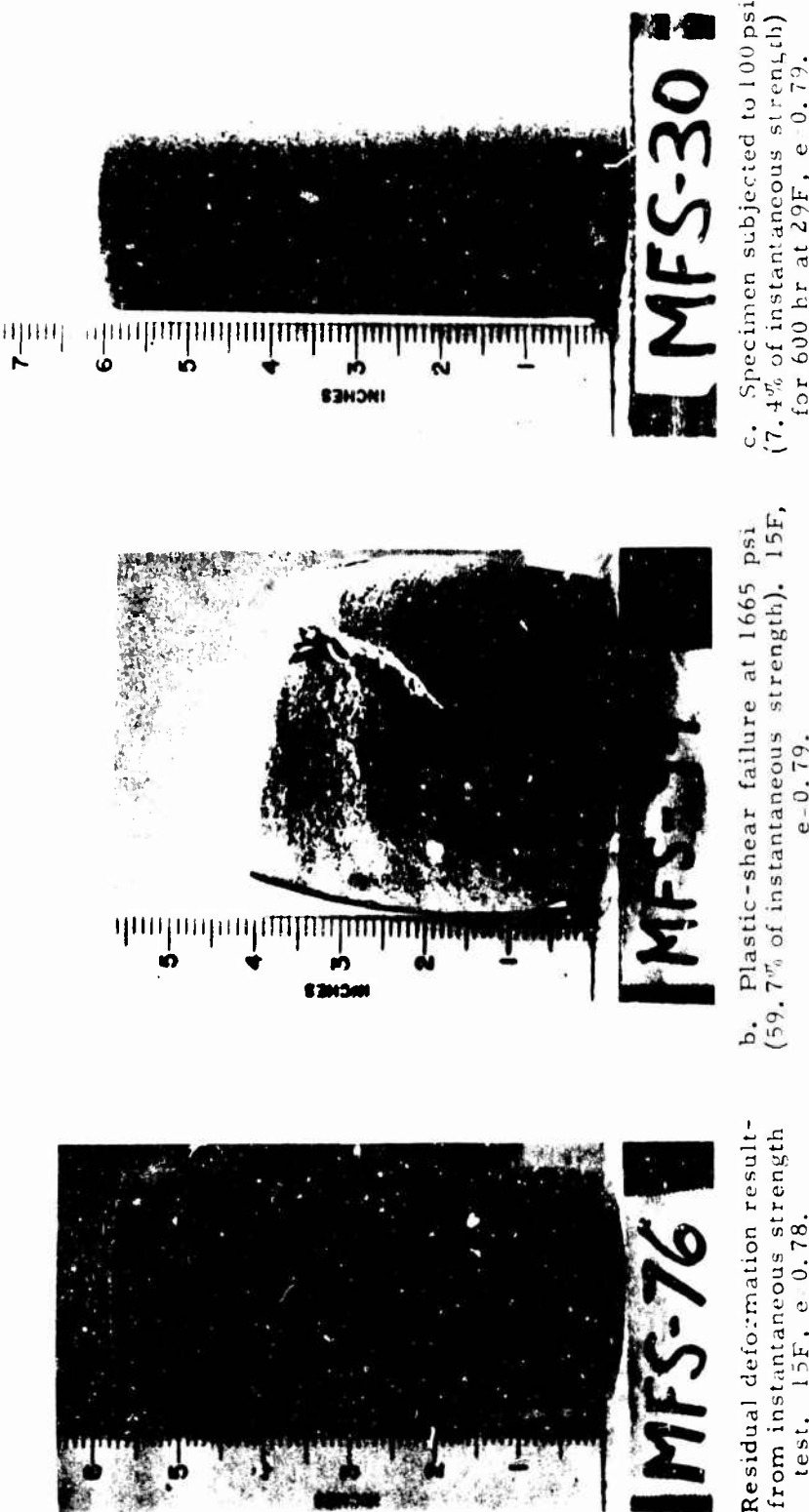


b. Plastic-shear failure at 815 psi (63.5% of instantaneous strength). Temp, 25F, $e=0.60$.



c. Specimen subjected to 200 psi (13.7% instantaneous strength) for 3500 hr at 25F; $e=0.60$.

Figure 11. Typical Ottawa sand specimens after testing.

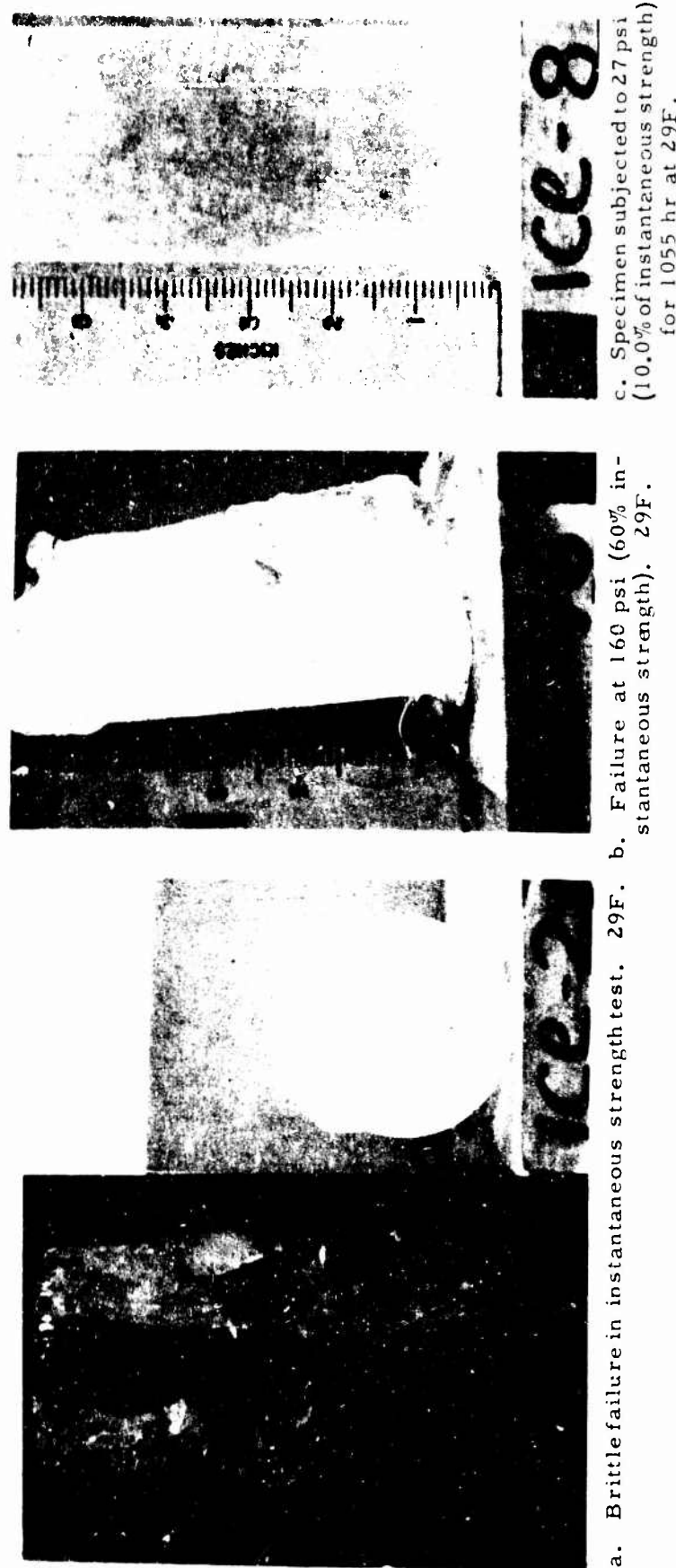


- a. Residual deformation resulting from instantaneous strength test. 15F, e 0.78.
- b. Plastic-shear failure at 1665 psi (59.7% of instantaneous strength). 15F, e 0.79.
- c. Specimen subjected to 100 psi (7.4% of instantaneous strength) for 600 hr at 29F, e 0.79.

Figure 12. Typical Manchester fine sand specimens after testing.

CREEP OF FROZEN SANDS

17



a. Brittle failure in instantaneous strength test. 29F. b. Failure at 160 psi (60% instantaneous strength). 29F. c. Specimen subjected to 27 psi (10.0% of instantaneous strength) for 1055 hr at 29F.

Figure 13. Typical ice specimens after testir 3.

CREEP OF FROZEN SANDS

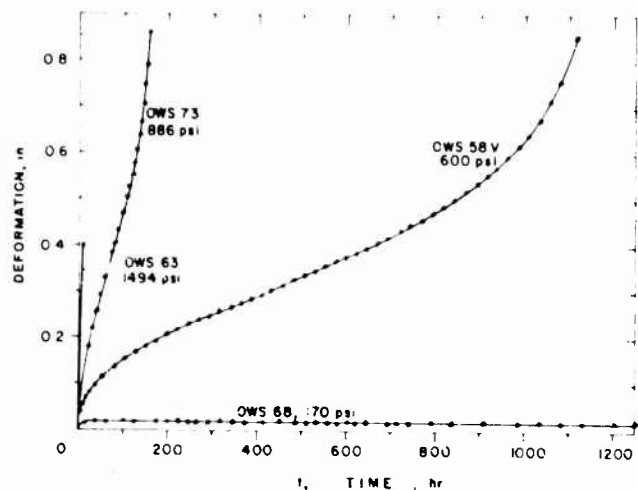


Figure 14. Creep tests in unconfined compression, Ottawa sand (20-30), 15F.

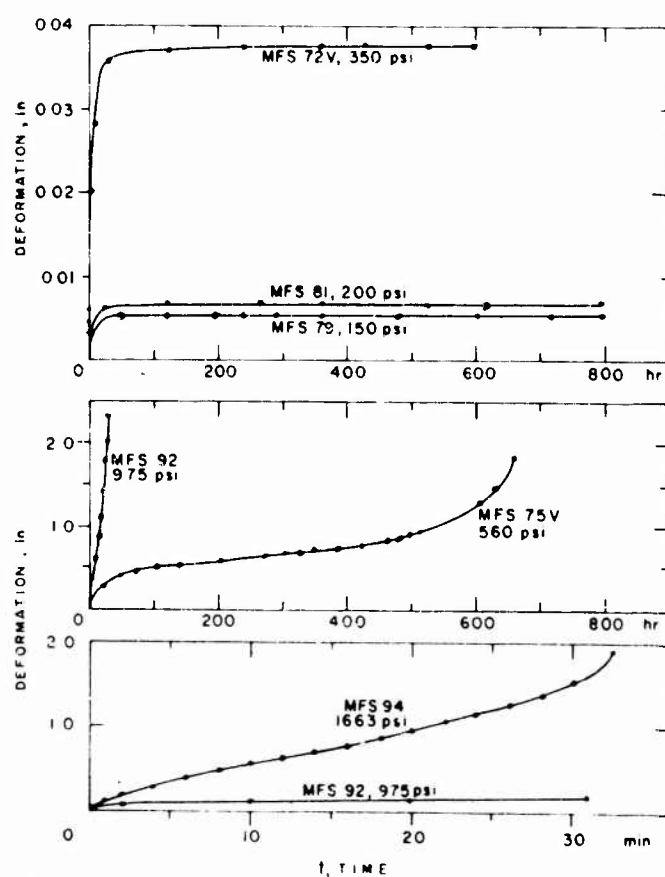


Figure 15. Creep tests in unconfined compression,
Manchester fine sand, 15F.

CREEP OF FROZEN SANDS

19

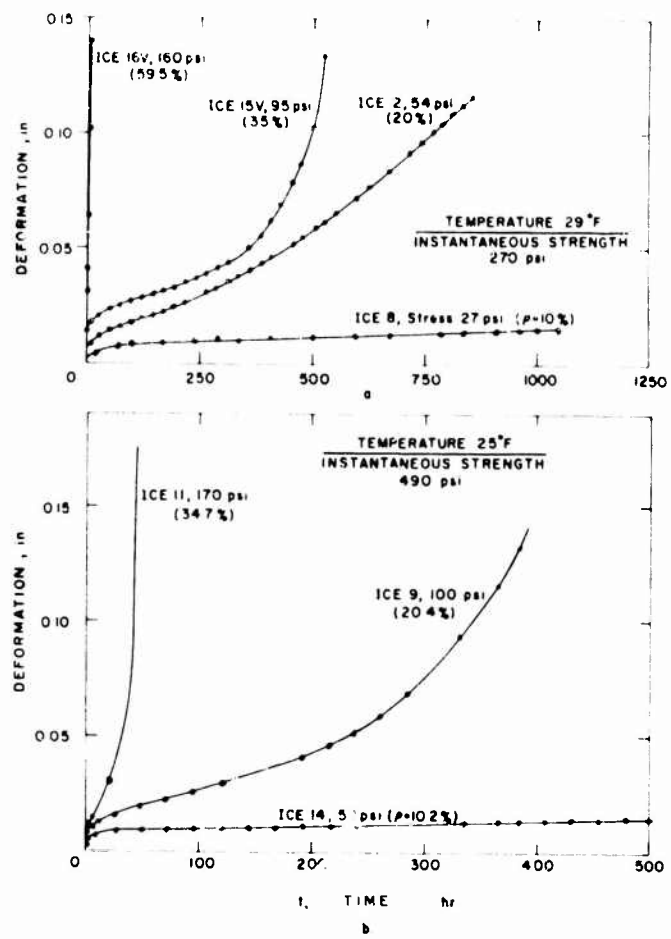


Figure 16. Creep test on ice in unconfined compression. ρ = stress ratio ($\frac{\text{test stress}}{\text{instantaneous strength}}$).

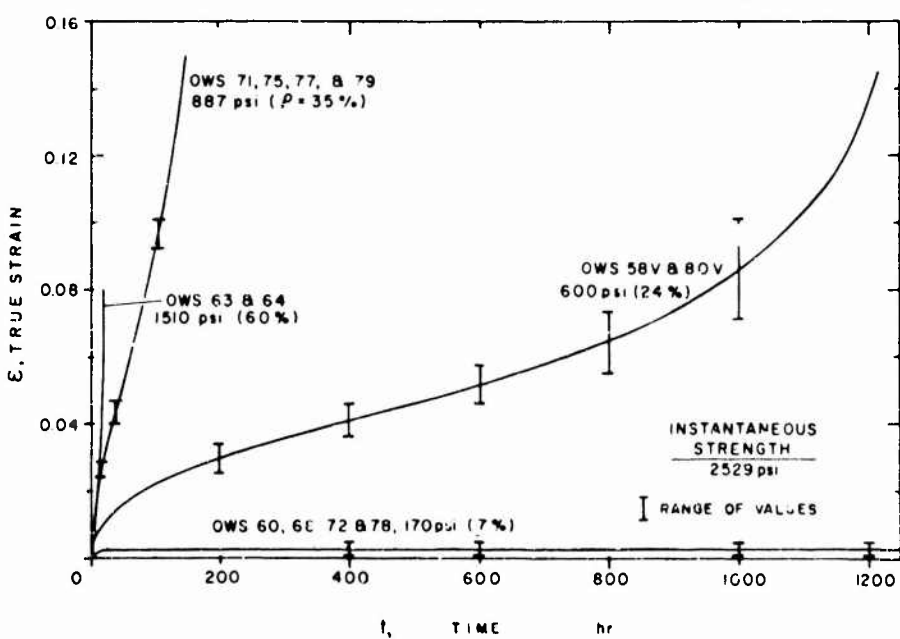


Figure 17. Time vs strain, Ottawa sand (20-30), 15F.

CREEP OF FROZEN SANDS

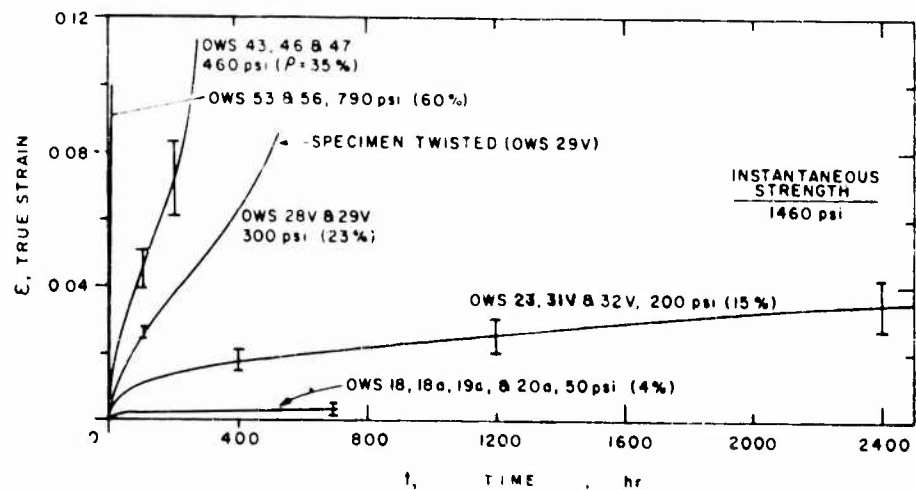


Figure 18. Time vs strain, Ottawa sand (20-30), 25F.

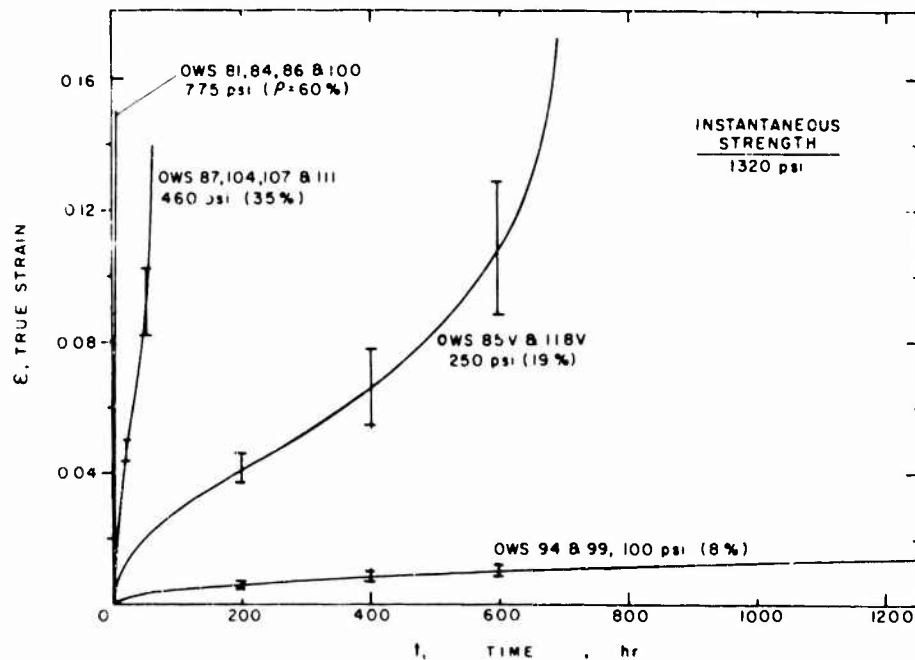


Figure 19. Time vs strain, Ottawa sand (20-30), 29F.

CREEP OF FROZEN SANDS

21

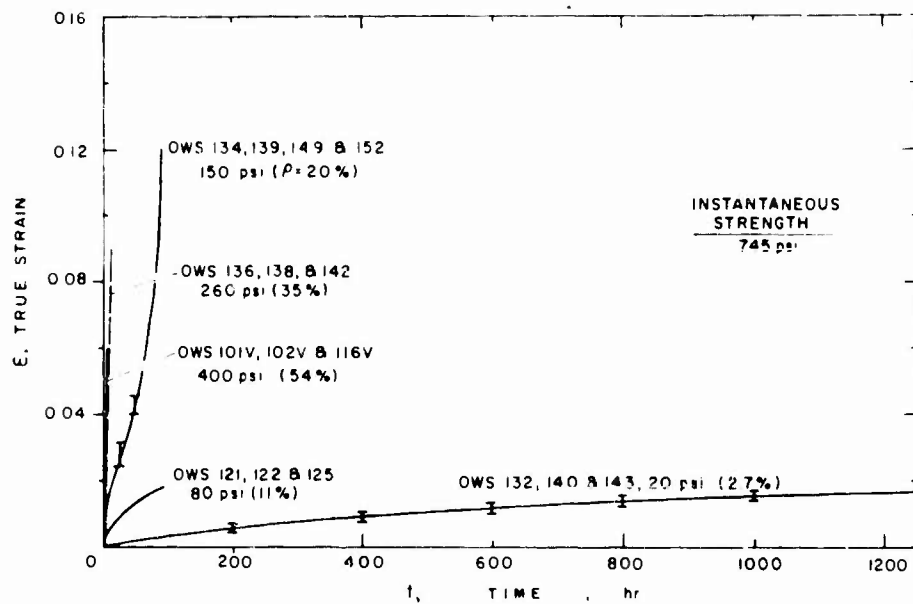


Figure 20. Time vs strain, Ottawa sand (20-30), 31F.

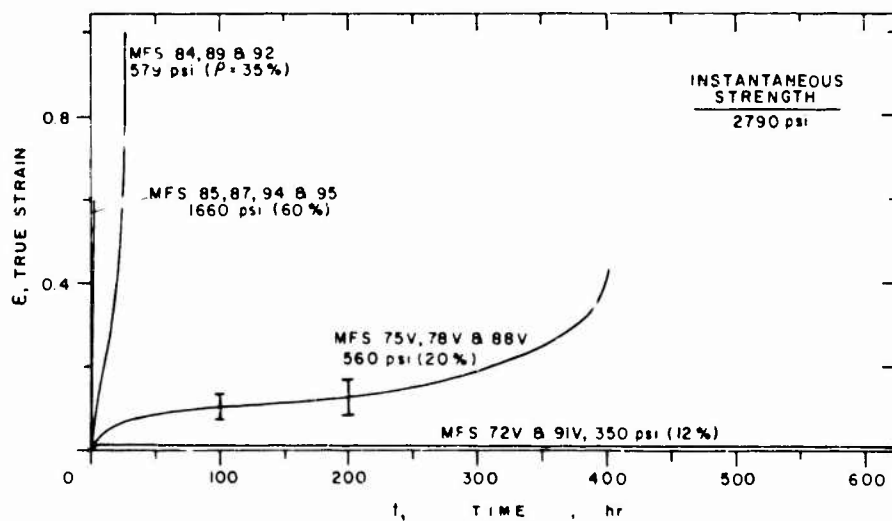


Figure 21. Time vs strain, Manchester fine sand, 15F.

CREEP OF FROZEN SANDS

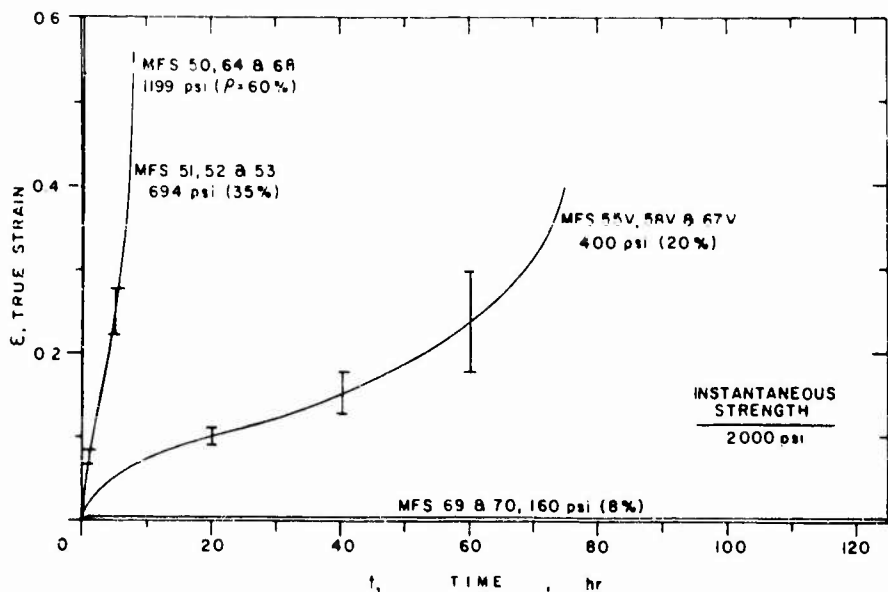


Figure 22. Time vs strain, Manchester fine sand, 25F.

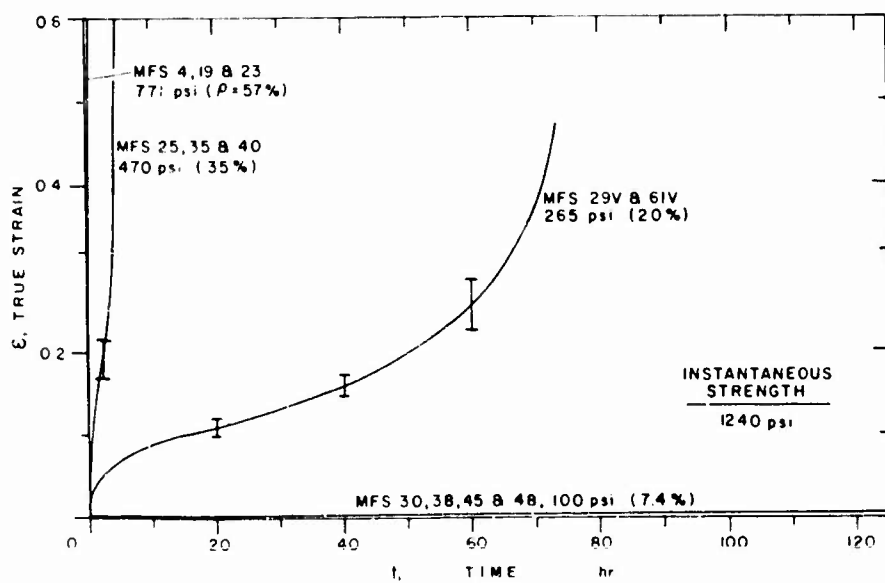


Figure 23. Time vs strain, Manchester fine sand, 29F.

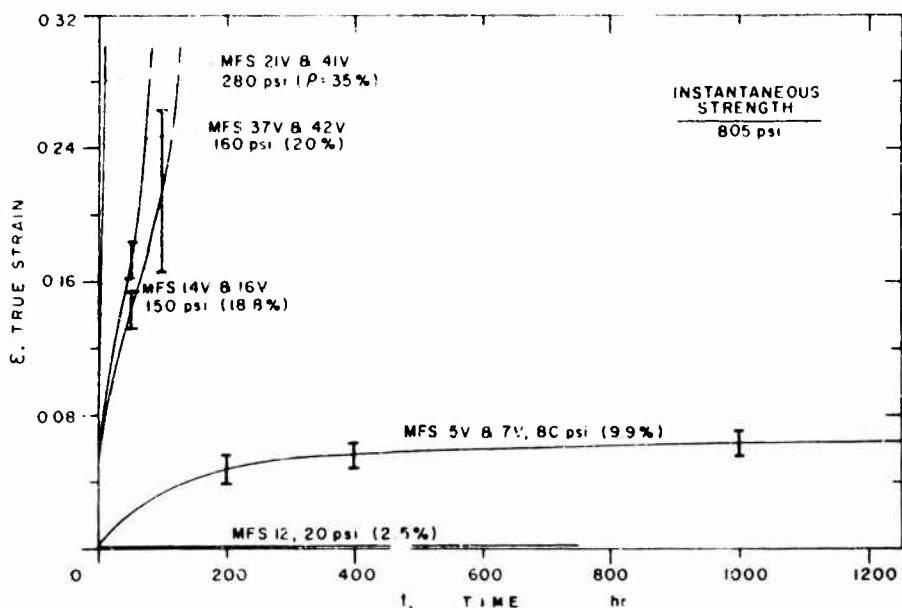


Figure 24. Time vs strain, Manchester fine sand, 31F.

DISCUSSION

Strain-time data

Creep data presented as deformation vs time curves are the primary results of this investigation and, with the exception of the "instantaneous" stress-strain curves, are the basis of all the curves reported herein. Typical time-deformation curves for sands are shown in Figures 14 and 15. From these curves, true ("logarithmic" or "natural") strains* were computed by subtracting test-machine calibration values from the deformations and adjusting the constant load test values to a constant stress basis. Typical time-strain curves are shown in Figures 17 - 24.

Deformation vs time, and strain vs time, curves for each temperature can be grouped according to shape. The curves for lower stress ratios (< 15%) show the rate of strain decreasing continuously with time and the total strain (or deformation) approaching a constant value asymptotically. Intermediate stress ratio (15 to 60%) curves are similar in shape to the classical creep curves shown in Figure 1 and exhibit large deformations prior to failure.† Curves for high stress ratios (> 60%) approach a straight line with relatively small deformations prior to failure. Figures 17 to 20 (Ottawa sand) and 21 to 24 (Manchester fine sand) are sets of average strain vs time curves showing the three differently shaped curves.

The low stress ratio group of curves consisting of instantaneous elastic, time-dependent elastic, and plastic components represents strains (or deformations) resulting from stresses smaller than the long-term strength† of the frozen soil. The various deformation components are labeled on the deformation rebound curve in Figure 25a. The total maximum long-term strain of the

* True strain = $\ln 1/(1-e_c)$ where the conventional strain $e_c = \Delta L/L_0 =$ axial deformation/original length.

† See page 1 for definition of terms.

CREEP OF FROZEN SANDS

specimens tested did not exceed 0.05 and 0.10 in./in. for Ottawa sand and Manchester fine sand, respectively. Ten rebound tests performed on frozen Ottawa sand indicate that the total elastic component is less than 15% of the total deformation and that the amount of instantaneous elastic deformation is generally less than time-dependent elastic deformations (see Table I). The percentage ranges of total deformations shown in Table I indicate that irreversible (plastic type) deformation is dominant even at stress levels below the long-term strength.

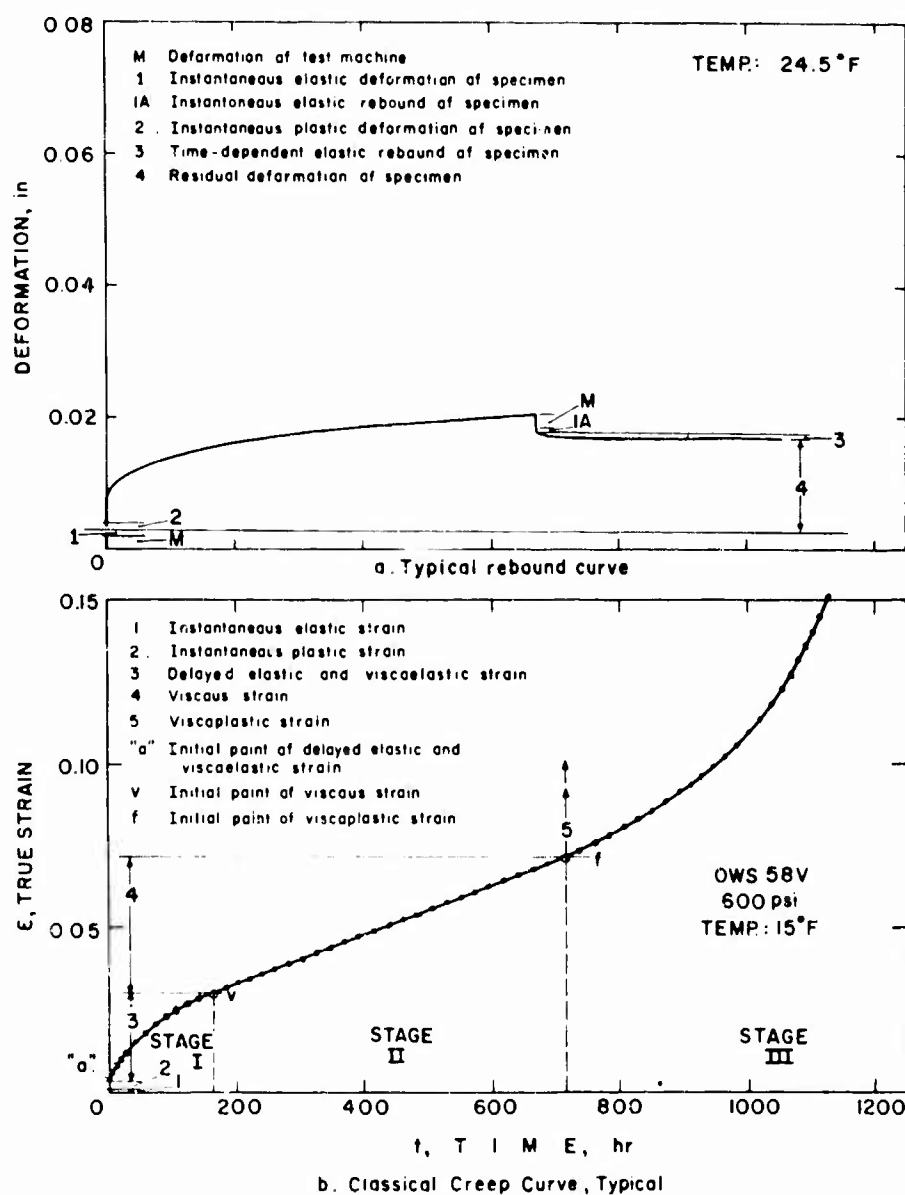


Figure 25. Typical rebound and classical creep curves, Ottawa sand (20-30).

Table 1. Types of deformations from rebounded creep tests, frozen Ottawa sand.

Temp (F)	Stress (psi)	Instant* rebound	Percent of Total Deformation			Rebound time observed (hr)
			Delayed elastic rebound	Total rebound	Plastic or plasto-viscous deform	
15	170	0 to 2.5	1.0 to 7	1.3 to 9	91 to 99	1/2
24.5	50	0 to 7	6 to 10	8 to 14	86 to 92	382
29	100	0 to 2	1 to 2	1 to 4	96 to 99	1

* Deformation observed 10 sec after removal of load.

At the intermediate stress ratios, the strain vs time curves display the characteristics of the classical creep curves for metals. These curves show instantaneous elastic and delayed elastic (i.e., viscoelastic), viscous, viscoplastic and plastic strains and eventual failure. In Figure 25b these components and the three creep stages are labeled on the time vs strain curve for an actual test specimen.

Strain components and strains at critical points are summarized in Table II. Section A of summary Table II shows: (1) that all instantaneous strains recorded (point a, Fig. 25b) are less than 0.6%; (2) that the range of strains where viscous flow begins (point v, Fig. 25b) is 0.3 to 4.7% for Ottawa sand and 3 to 15% for Manchester fine sand; (3) that the range of strains at initial viscoplastic flows (point f, Fig. 25b, start of tertiary creep) are 0.6 to 8.0 and 12 to 28% for Ottawa sand and Manchester fine sand, respectively. It should be noted that the larger strains experienced by Manchester fine sand under equivalent conditions could be explained by the greater void ratio of these specimens.

The magnitudes of each of the strain components in percent, compared in Section B of Table II, do not reveal an obvious trend but do indicate that the viscoelastic component (strain component 3, Figure 25b), and the viscous component (strain component 4, Figure 25b) are roughly of the same order of magnitude and that the instantaneous strain is insignificant in comparison.

Section C of Table II compares the three strain components as percentages of the total strain experienced by test specimens prior to the onset of final viscoplastic strain (i.e., as percent of the strain at point f). At each temperature in this tabulation, the viscous component of the Manchester fine sand curve tends to increase and, correspondingly, the initial viscoelastic components tend to decrease as the stress increases. This trend does not necessarily mean that the viscoelastic component is smaller but that it can be obscured by the more stress-sensitive viscous component. Rebound creep tests at the higher stress levels would help clarify this point. Plots showing these trends are given in Figures 26a and 26b. No similar trends were detected in the Ottawa sand data, possibly because the smaller void ratio of the Ottawa sand permits less viscous flow of the ice matrix in the sand voids prior to the development of greater frictional resistance between the sand grains.

It was noted for stresses greater than the long-term strength that viscous type deformation was observed early in the tests, an observation that permits an early prediction of eventual specimen incipient failure and failure.* Failure occurred by either an abrupt brittle-type fracture (Fig. 11a) or a plastic flow accompanied by fissuring (Fig. 11b and 12b). The plastic-flow type failure occurred after large deformations, and fissures often preceded the abrupt collapse of the specimen.

* See p. I for definition of terms.

CREEP OF FROZEN SANDS

Table II. Strain components and strain at critical points under intermediate stresses (see Fig. 2b).

Temp °F	Stress psi	Strength % of instant. Strength	SECTION A			SECTION B			SECTION C		
			% Strain at critical points on creep curves			Components of strain in percent			Components of strain % of strain at point <i>f'</i>		
			Stress as % of instant. Strength	'a'	'b'	'c'	'd'	'e'	'f'	'g'	'h'
OTTAWA SAND (20-30)											
15	600	24	0.07-0.13	3.4-1.9	4.6-6.3	0.37-0.13	3.0-4.0	0.7-3.0	1.6-2.1	54-83	16-45
	887	35	0.09-0.13	4.1-4.3	6.1-7.2	0.09-0.13	3.7-4.2	2.0-3.1	1.4-1.9	56-66	32-43
	1510	59	0.05-0.08	0.3-4.1	0.6-0.7	0.05-0.08	0.2-0.3	0.3-0.4	8.0-12	37-72	47-56
25	460	32	0.01-0.12	3.9-4.6	5.8-7.2	0.01-0.12	3.8-4.4	1.8-2.0	1.0-2.0	53-70	28-46
	790	54	0.1-0.09	0.7-1.1	5.7-6.3	0.01-0.09	0.7-1.0	4.9-5.2	0.1-0.2	12-16	82-87
29	250	19	0.06-0.22	2.8-3.4	5.7-6.1	0.06-0.22	2.7-3.2	2.7-2.9	1.0-4.0	48-53	44-50
	460	35	0.06-0.15	3.3-3.6	7.0-7.7	0.06-0.15	3.4-3.6	7.0-7.6	0.8-2.0	42-49	50-53
	775	59	0.05-0.20	3.9-4.7	7.4-8.1	0.05-0.20	3.6-4.6	3.4-3.8	4.6-5.0	46-57	42-51
31	150	20	0.10-0.12	1.5-1.9	4.8-5.1	0.10-0.12	1.4-1.8	3.0-3.3	2.0-3.0	52-55	62-68
	260	35	0.06-0.08	1.0-1.6	2.7-3.5	0.06-0.08	0.9-1.3	1.7-2.5	1.0-3.0	26-33	55-62
	400	54	0.17-0.24	0.8-1.5	1.7-4.6	1.17-0.24	0.6-1.3	0.9-3.2	5.0-11	27-37	53-69
MANCHESTER FINE SAND											
15	560	20	0.05-0.20	8-11	1.2-17	0.05-0.20	8-11	4-6	0.3-1.1	64-69	34-40
	976	35	0.10-0.40	12-15	2.1-28	0.10-0.40	12-15	10-13	0.4-1.6	52-55	44-47
	1660	60	0.16-0.60	3-7	1.3-17	0.15-0.60	3-7	8-13	1.0-3.7	21-45	56-79
25	400	20	0.09-0.15	7-9	1.3-16	0.09-0.15	6-9	5-9	2.6-1.1	43-61	38-57
	694	35	0.05-0.45	10-11	2.2-24	0.05-0.45	10-11	12-13	0.2-1.8	43-46	54-55
	1199	60	0.01-0.40	7-12	2.2-25	0.01-0.40	6-12	14-18	0.5-1.7	30-43	56-72
29	265	20	0.15-0.17	8-11	1.3-15	0.15-0.17	8-11	4-5	1.0-1.3	64-69	30-35
	470	35	0.14-0.20	9-11	1.7-21	0.14-0.20	9-11	7-11	0.8-1.1	47-58	41-52
	771	57	0.23-0.31	9-10	2.4-27	0.23-0.31	8-10	14-17	0.9-1.3	35-37	62-64
31	150	19	0.06-0.10	11-12	1.5-18	0.06-0.10	11-12	3-7	0.3-0.6	65-77	22-35
	160	20	0.10-0.12	9-10	1.7-20	0.10-0.12	9-10	7-10	0.5-0.7	51-56	42-49
	280	35	0.20-0.30	10-12	1.9-20	0.20-0.30	10-12	7-9	1.3-1.4	52-59	39-47

High stress ratio curves exhibit an abbreviated form of the classical creep curve passing rapidly through the three stages of the creep curve and terminating in an abrupt failure.

It should be noted that the deformation curves for ice (Fig. 16a, b) exhibit the same general types of curves corresponding to each of the three stress ratios for the frozen sands except that low stress ratios in ice produced undamped viscous deformation (i. e., a constant rate of deformation) rather than damped deformation exhibited by the sand. Glen (1955), Jellinek and Brill (1956) and Butkovich and Landauer (1959, 1960) investigated creep and viscoelastic properties of ice under low stress and have formulated theories and equations describing its behavior as influenced by stress, temperature and structure. Tests on ice in the present investigation were conducted solely for comparison with similar tests on frozen sand under the same test conditions.

Strain rate

Rates of strain were determined as the slopes of the strain vs time curves using a digital computer.* The rates for each test specimen were computed by considering successive groups of five consecutive data points on the strain vs time curves. A second degree polynomial equation was fitted to the five data points by the method of least squares, then the slope of the equation was determined at the middle point of the five data points. New groups of five data points were considered by advancing along the strain vs time curve one point at a time (i. e., by eliminating the first data point and including a new advanced data point). The process of fitting the polynomial equation and determining the slope of the equation was repeated for each group of five data points. Using this system, rates of strain were determined for the entire length of the strain vs time curve except for the first two and last two points on the curve. The procedure was readily adapted to digital computer methods and by considering only five points at a time it was not necessary to determine an expression for the entire strain-time curve.

Typical strain rate vs time curves for both the damped and undamped type creep tests are plotted on Figure 27. The undamped curve has a high initial strain rate which decreases hyperbolically (during creep stage I) to a minimum relatively constant value (creep stage II or viscous flow), then increases rapidly (creep stage III) until specimen failure. The initial portion of the damped curve is similar in shape to the undamped curve except that it approaches a zero strain rate.

Typical strain-rate vs reciprocal-of-time curves for three applied stresses plotted on log coordinates (Fig. 28) show that the strain rates of both the damped and undamped creep curves are initially straight lines. The undamped curve represented by the 260 psi curve reaches a minimum strain rate then increases rapidly as indicated by the sharp turn to the right. In contrast the damped curve remains a straight line then decreases (i. e., turns to the left) as the rate of strain approaches zero (see Fig. 29). Although the 20 psi curve on Figure 28 is for a damped creep test, it does not show the decrease in creep rate as clearly as the damped curves on Figure 29. One possible explanation for this decrease in strain rate can be that friction between sand grains increases enough to dominate the creep of the test specimen and eventually produce stability.

* The method of determining strain rates was suggested by Dr. A. Assur, Chief Scientist, USA CRREL.

CREEP OF FROZEN SANDS

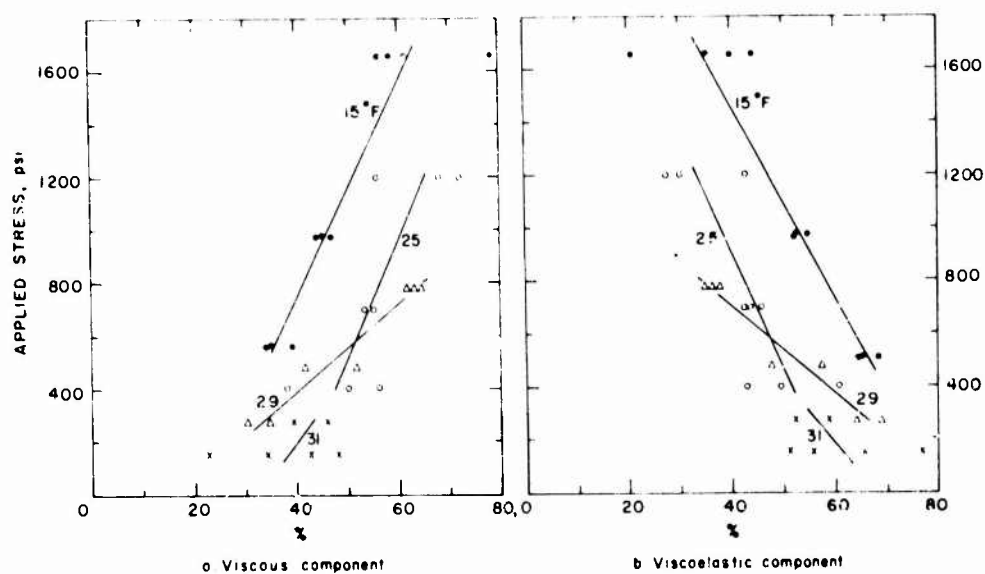


Figure 26. Percent of strain at start of tertiary creep, Manchester fine sand, various temperatures.

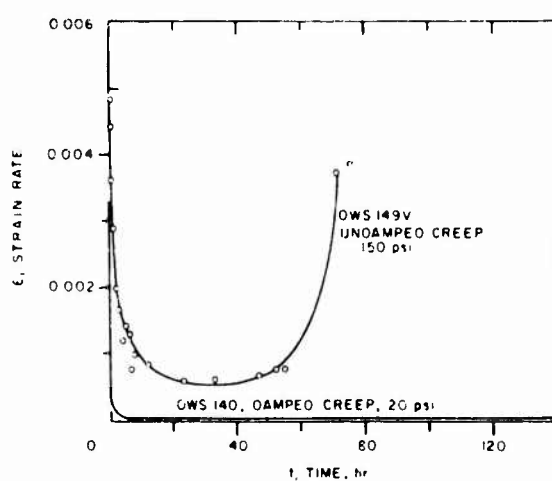


Figure 27. Creep rate and time, Ottawa sand (20-30), 31°F.

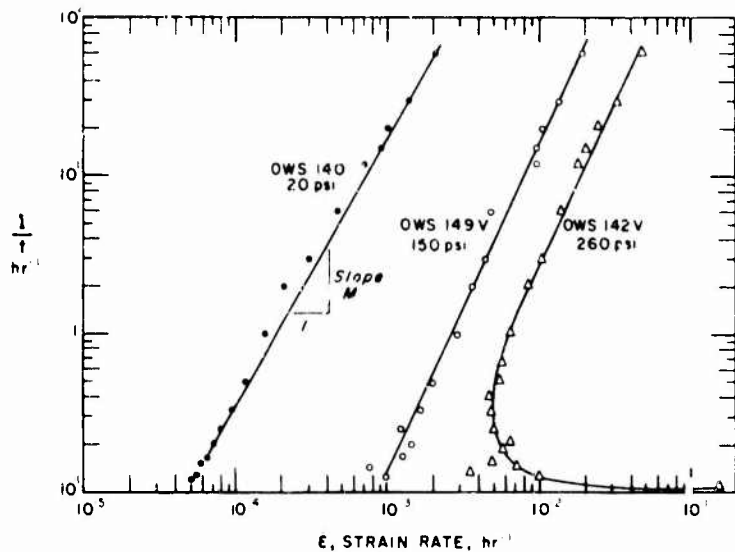


Figure 28. Creep rate and reciprocal of time, Ottawa sand, 31F.

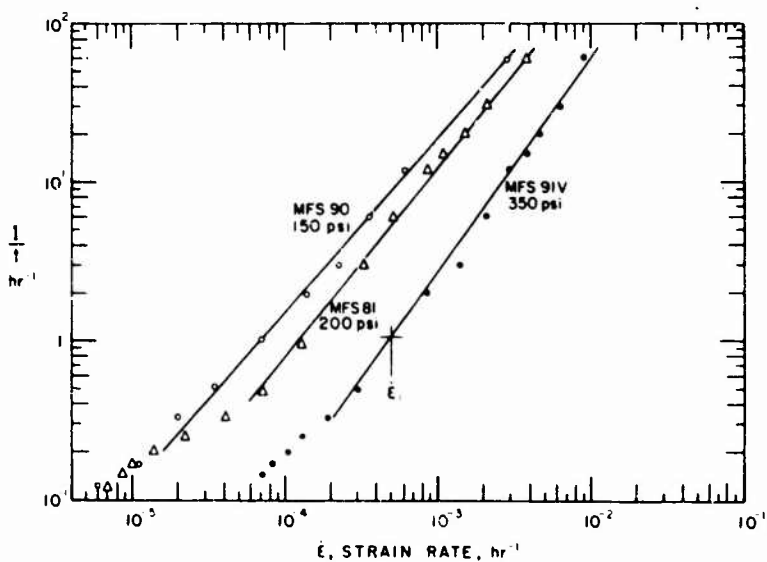


Figure 29. Creep rate and reciprocal of time, Manchester fine sand, 15F.

The three damped curves on Figure 29 for the constant temperature of 15F indicate that not only the magnitude of the strain rate but also rate of change of the strain rate (i.e., the slope of the curve) is stress dependent. Since the slope is steeper for higher stresses, the creep decelerates faster and stabilizes faster for the higher damping stresses.

By comparing the 15F and 25F curves of Figure 30, it is clear that at increased temperatures the rate of strain is increased. The 10 psi difference in test stresses between the two curves produces a relatively minor change at the temperatures involved. A similar comparison between the 29F and 31F curves (Fig. 30) shows that the rate of decrease in strain rate is greater at the higher

CREEP OF FROZEN SANDS

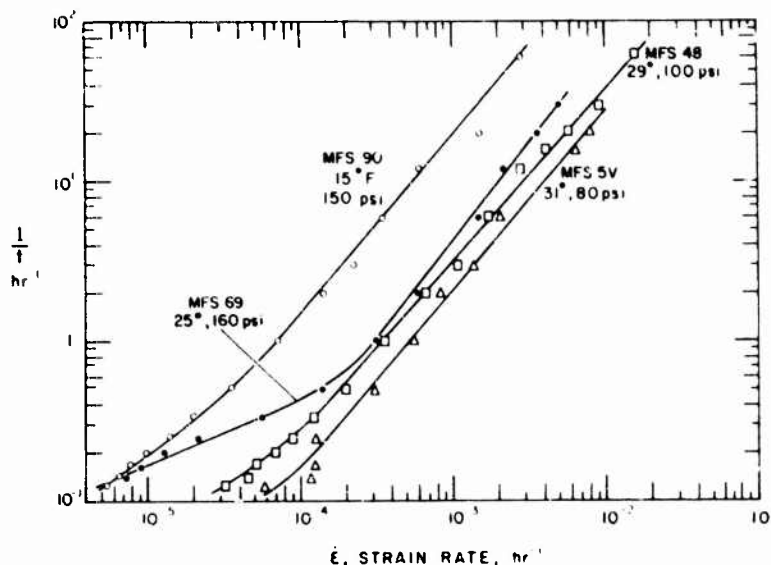


Figure 30. Creep rate and reciprocal of time, Manchester fine sand at various temperatures.

test temperature even though the stress is smaller (i.e., the slope is greater at the higher temperature). This indication of deceleration of creep with increased temperature requires further investigation since only a trend was noticed here.

Strain equations

An equation to be used for the prediction of the creep strain of a given frozen soil must at least include factors that reflect the influence of the soil temperature, the magnitude of the applied stress, the time during which the stress acts, the ice or water content, the soil particle size and the density. Although other factors affect the creep strain, their influence is reflected indirectly by these factors listed.

Strain equation by Vialov. S. S. Vialov (1962) has presented a creep strain equation based on tests performed on undisturbed sandy silt and clay, which includes the most essential factors either directly or indirectly. Vialov's equation for total strain is:

$$\epsilon = \left[\frac{\sigma t^\lambda}{\omega(\theta + 1)^k} \right]^{1/m} + \epsilon_0 \quad (1)$$

where: σ = applied constant stress kg/cm^2
 t = time, hr
 θ = temperature in degrees C below the freezing point of water
 ϵ_0 = instantaneous strain
 λ, m, ω and k = constants that are characteristic of the material (and ω depends on units).

This equation conceals the fact that $\ln(1+\theta)$, the 1 has temperature units. For this reason, Assur (1963) suggested that the equation be written:

$$\epsilon = \left[\frac{\sigma t^\lambda}{\omega(\theta + \theta_0)^k} \right]^{1/m} + \epsilon_0 = \left[\frac{\sigma t^\lambda}{\omega \theta_0^k (\frac{\theta}{\theta_0} + 1)^k} \right]^{1/m} + \epsilon_0. \quad (1A)$$

Here, the numerical values of m and λ do not, but ω and θ_0 do, vary with the units employed. θ_0 = an assumed constant reference temperature greater than zero. Vialov assumed $\theta_0 = 1^\circ C$ so that $\lg(1+\theta)$ had meaning at $\theta = 0$. In this report $\theta_0 = 1^\circ F$ was used. For numerical comparisons, stress, time and temperature data should be converted to the same units.

The first term on the right side of this equation was developed from the power function relationship, $\sigma = A \epsilon^m$, between stress and strain for stresses less than the long-term strength of the test material, where $A = f(\theta, t)$, in the units of stress.

Values for A and m are obtained from log plots of stress against strain (see Fig. 31a, b) for various time intervals after stress application to the test specimens. Vialov represented sandy silt and clay data by a straight line on a $\log \sigma$ vs $\log \epsilon$ plot even though he recognized that a curve did exist. The sand data reported herein also showed some curvature. This curvature along with the experimental scatter made it difficult to represent the $\log \epsilon$ vs $\log \sigma$ curves as straight lines. However, to determine the constants in Vialov's strain equation for the sand data, straight lines were drawn as indicated in Figures 31a and b for all test data. The average slopes of these curves (m) are shown in Table III. This table indicates that within the accuracy of the tests, the values of m are independent of temperature for both the Ottawa sand and the Manchester fine sand. m may be considered a characteristic of the material and its density, and its value is independent of the units employed.

Table III. Value of m in Vialov's strain equation.

Temperature °F	Ottawa sand	Manchester fine sand
15	0.78	0.42
25	0.79	0.36
29	0.77	0.40
31	0.79	0.35
Average	0.78	0.38

Table IV. Constants for Vialov's strain equation.

Material	m	λ	ω	k	ω	k
			For $\theta_0 = 1^\circ F$	[psi(hr) $^\lambda$] / °F k	For $\theta_0 = 1^\circ C$	[psi(hr) $^\lambda$] / °C k
Ottawa sand (20-30 mesh)	0.78	0.35	5500	0.97	3600(456)†	1.0
Manchester fine sand (40-200 mesh)	0.38	0.24	285	0.97	185(23.4)	1.0
Silt* (Callovian sandy loam)	0.27	0.10	90	0.89	76(9.0)	0.89
Clay* (Bat-Baioss clay)	0.4	0.18	130	0.97	103(12.8)	0.97

* Data from Vialov et al. (1962), Chapter V.

† ω in $\text{kg/cm}^2 \text{ hr}^\lambda / {}^\circ \text{C}^k$ shown in parentheses.

CREEP OF FROZEN SANDS

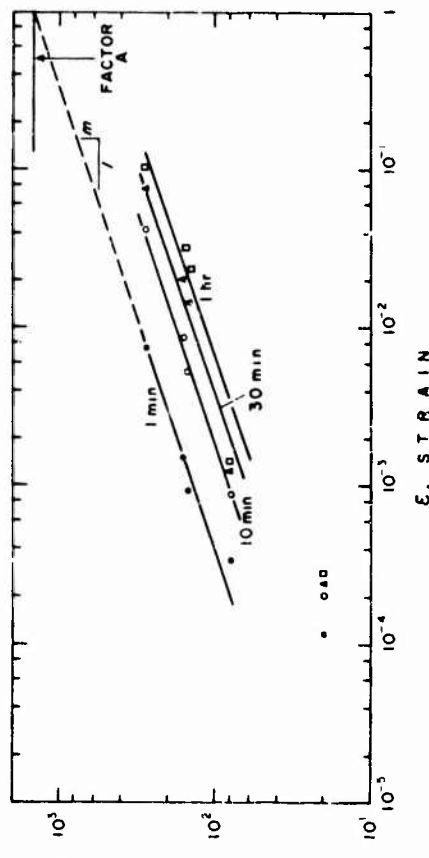
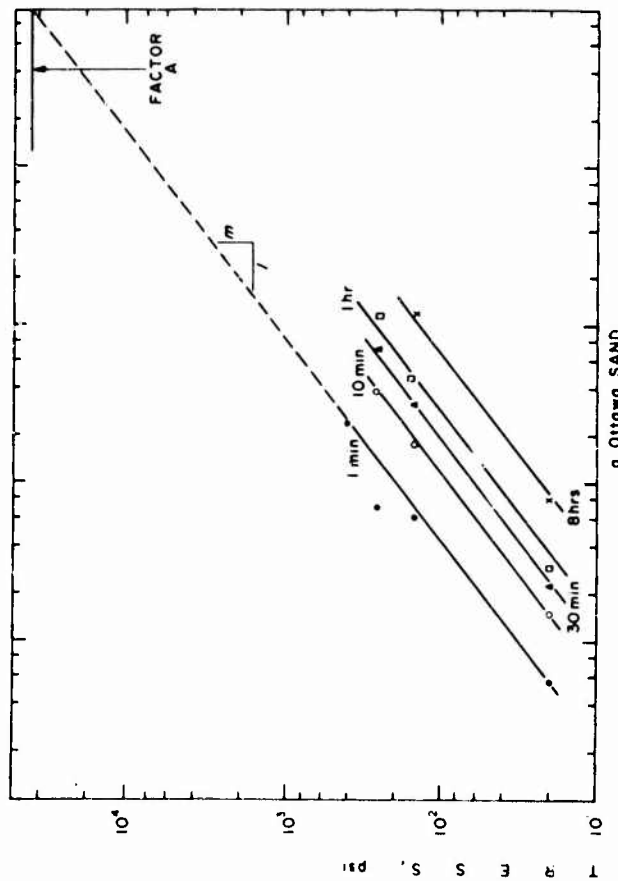


Figure 31. Stress, strain and time, 31F. $\sigma = A \epsilon^m$.

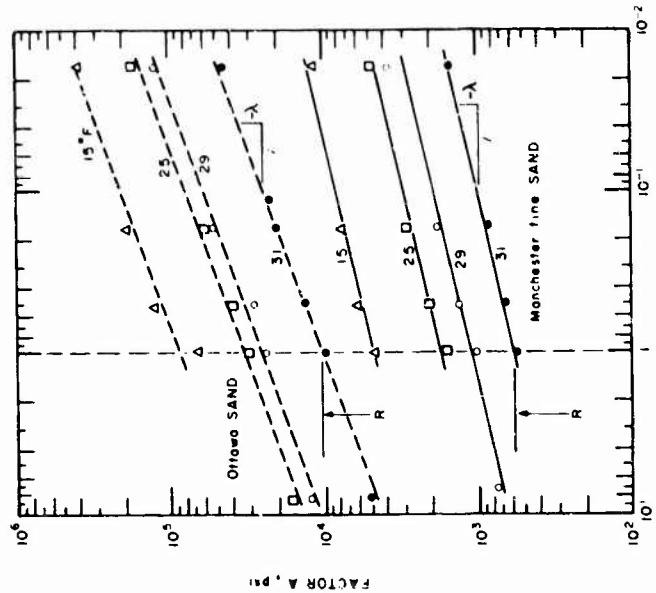


Figure 32. Time, factor A, and temperature.

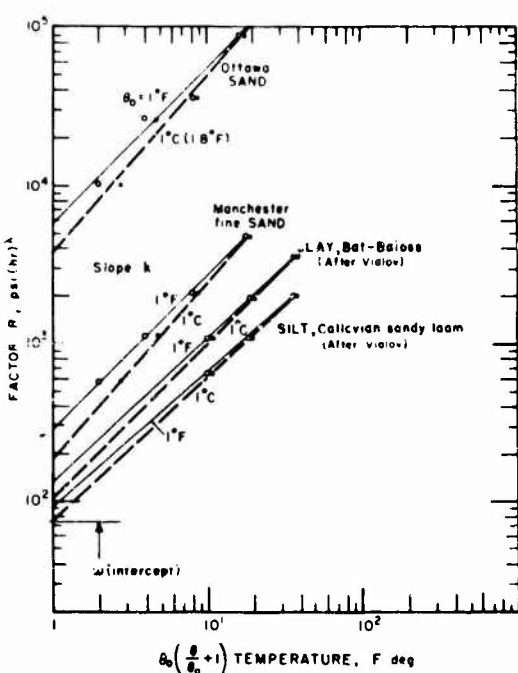


Figure 33. Factor R and temperature.

strain rates where only the differences in strain (i.e., deformation) need to be measured. Like Vialov's equation the only stress condition under consideration is where the applied stress is less than the long-term strength (i.e., for damped creep tests) and the instantaneous strain is neglected.

The straight line portion of the $\log(1/t)$ vs \log strain rate curves for damped creep tests on Figures 28 to 30 can be represented by:

$$\frac{1}{t} = \left[\frac{\dot{\epsilon}}{\dot{\epsilon}_1} \right]^M \quad \text{or} \quad \dot{\epsilon} = \dot{\epsilon}_1 t^{-1/M}.$$

By integration

$$\epsilon = \dot{\epsilon}_1 \left(\frac{M}{M-1} \right) t^{\frac{(M-1)}{M}} + \epsilon_0 \quad (2)$$

where: ϵ = strain
 $\dot{\epsilon}$ = strain rate
 $\dot{\epsilon}_1$ = strain rate 1 hour after stress is applied
 ϵ_0 = initial instantaneous strain as stress is applied
 t = time after stress is applied
 M = slope of $\log 1/t$ vs \log strain rate.

An examination of the strain rate curves (Fig. 30) reveals that M is a function of both temperature and stress, but for the temperature range investigated, the stress effect predominates. Assuming M is independent of temperature, and is a straight line function of stress on logarithmic coordinates (Fig. 35), the equation for M becomes:

$$M = C \sigma^{1/w} \quad (3)$$

By plotting A (i.e., the ordinates for log strain equal to unity) from Figures 31a and b against time for the different test temperatures, values for factor $R (= At^\lambda)$ and exponent λ were obtained as shown on Figure 32. The constants w and k were similarly obtained by plotting the intercept R against $\theta_0 (\frac{\theta}{\theta_0} + 1)$ as shown on Figure 33. The values for Ottawa sand and Manchester fine sand are listed in Table IV along with those for sandy silt and clay published by Vialov (1962).

Figures 34a and b show a comparison between Vialov's equation and actual test data for Manchester fine sand and Ottawa sand, respectively.

Strain equation based on strain rate. Vialov's equation demands quite precise measurements of the absolute values of strain (i.e., deformation) and also requires several tests for the evaluation of the formula constants. To overcome these two difficulties and to provide a more flexible approach, a strain equation was developed using

CREEP OF FROZEN SANDS

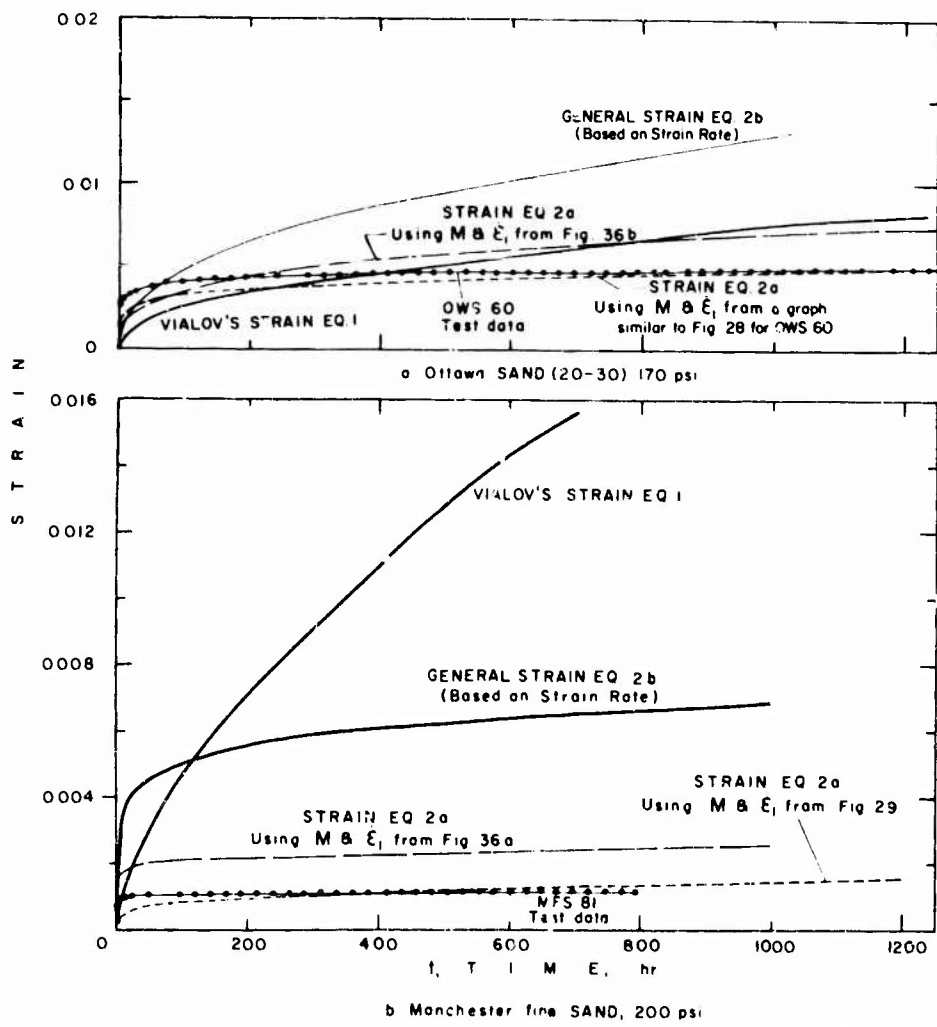


Figure 34. Strain and time - comparative curves, 15F.

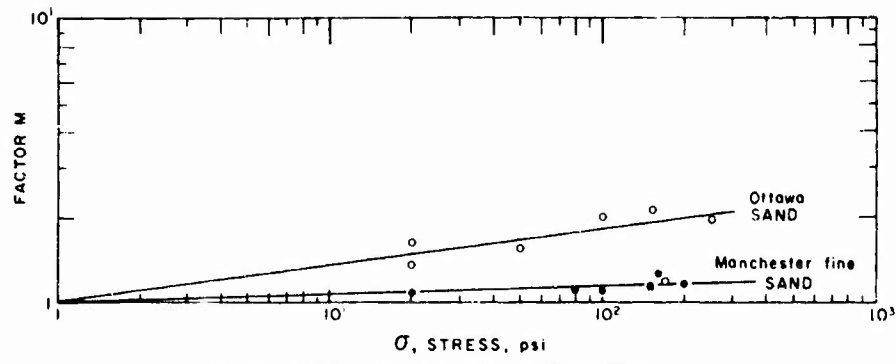


Figure 35. Factor M and stress.

CREEP OF FROZEN SANDS

35

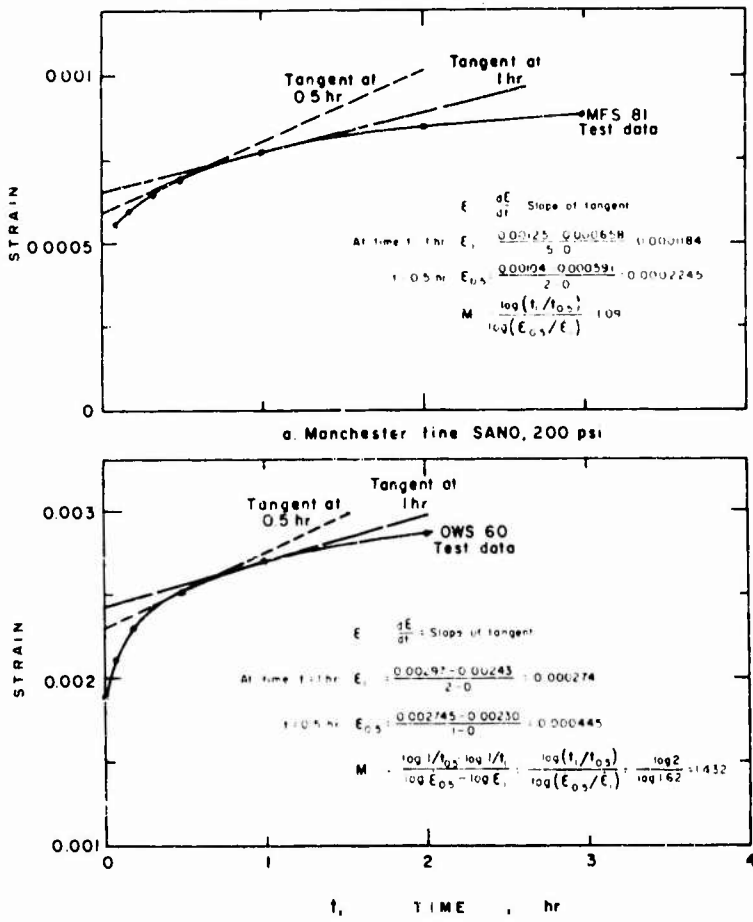


Figure 36. Strain and time, 15F.

where w is the slope of $\log \sigma$ vs $\log M$ curve and treated as a constant for each material. Values of w determined graphically for the Ottawa sand and Manchester fine sand at the densities tested are 9 and 35, respectively, and C is almost exactly unity for each sand.

The values of $\dot{\epsilon}_1$ and M in eq 2 can be determined graphically using the slopes of the tangent to the strain vs time curve on arithmetic coordinates at times of $\frac{1}{2}$ hour and 1 hour after stress application (Fig. 36a, b) or by using the $\log \dot{\epsilon}$ vs $\log 1/t$ curves for the first 8 hours of the creep test data (see Fig. 29). The arithmetic coordinate method offers a simple, rapid means for predicting strain but is not as accurate as the method using the $\log \dot{\epsilon}$ vs $\log 1/t$ curves. The logarithmic coordinate method predicts long-term strains that are in close agreement with the actual data; however, the method requires the determination of the strain rates at several points on the 8-hour time-strain curve. These strain rates can be found graphically by drawing tangents as indicated in Figures 36a and b or by fitting a polynomial expression to a portion of the strain-time curve and then differentiating it, a method that was used to obtain the strain rates in Figures 29 and 30. Strain curves predicted by eq 2 using both arithmetic coordinates and logarithmic plotting for determining $\dot{\epsilon}_1$ and M are compared with test data on Figures 34a and b.

A more general expression for $\dot{\epsilon}_1$ can be obtained by representing the logarithmic plots of $\dot{\epsilon}_1$ vs σ for each temperature by a straight line as shown in Figures 37a and b. The general equation for each temperature is:

CREEP OF FROZEN SANDS

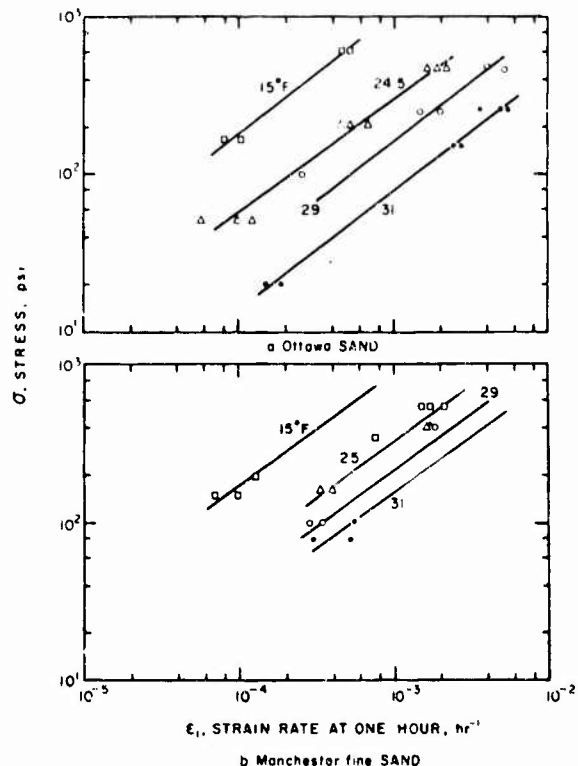


Figure 37. Strain rate at time 1 hr, and stress. Various temperatures.

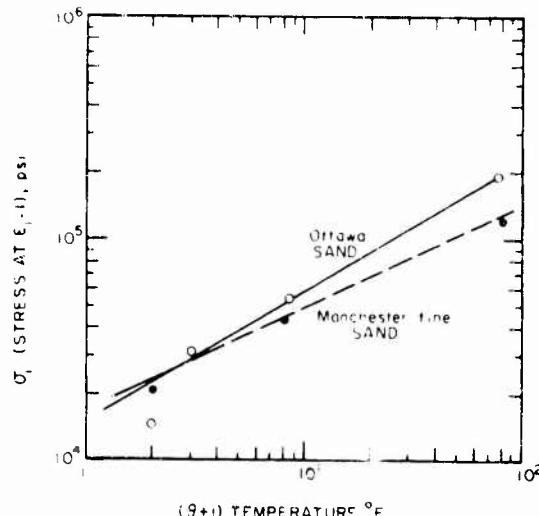


Figure 38. Temperature and stress σ_1 for unit strain rate at 1 hr ($\dot{\epsilon}_1$).

$$\begin{aligned} \sigma &= \sigma_1 \dot{\epsilon}_1^K \\ \dot{\epsilon}_1 &= \left(\frac{\sigma}{\sigma_1} \right)^{1/K} \end{aligned} \quad (4)$$

where σ_1 = stress at which $\dot{\epsilon}_1$ is unity
 K = constant slope of the straight line plot.

This equation assumes that σ_1 is temperature dependent, and that K is constant for the materials and the temperature range investigated (as indicated by the parallelism of the lines).

Temperature and σ_1 are plotted on Figure 38. [The quantity $(\theta + 1) = \theta_0 \left(\frac{\theta}{\theta_0} + 1 \right)$ was used instead of θ to avoid the logarithm of zero at a temperature of 32°F.]

The equation for each straight line on Figure 38 is:

$$\sigma_1 = \sigma_{01} (\theta + 1)^a \quad (5)$$

where σ_{01} is stress at $\theta = 0$ (temp 32°F)
 a (const.) is slope of the straight line plot.

By substituting the expression for σ_1 into eq 4, an expression for $\dot{\epsilon}_1$ is:

$$\dot{\epsilon}_1 = \left[\frac{\sigma}{\sigma_{01} \theta_0^a \left(\frac{\theta}{\theta_0} + 1 \right)^a} \right]^{1/K} \quad (6)$$

or

$$\dot{\epsilon}_1 = \left[\frac{\sigma}{\sigma_{01} (\theta+1)^a} \right]^{1/K} \quad (6a)$$

where θ is in Fahrenheit degrees.

Using $\psi = \frac{M-1}{M}$; eq 2 becomes

$$\epsilon = \dot{\epsilon}_1 \frac{t\psi}{\psi} + \epsilon_0 \quad (2a)$$

and substituting $\dot{\epsilon}_1$ from eq 6, then

$$\left[\frac{\sigma}{\sigma_{01} \theta^a (\frac{\theta}{\theta_0} + 1)^a} \right]^{1/K} \frac{t\psi}{\psi} + \epsilon_0$$

or

$$\epsilon = \left[\frac{\sigma}{\sigma_{01} (\theta + 1)^a} \right]^{1/K} \frac{t\psi}{\psi} + \epsilon_0 \quad (2b)$$

On Figures 34a and b, eq 2a and b (neglecting ϵ_0) are compared with Vialov's equation and the test data. Equation 2a has the advantage of requiring only a single short-term creep test to predict the total strain for a given material after applying a stress for a specified time. Equation 2b can be used to estimate total strain where only the general type soil (i.e., coarse sand, fine sand, silt, clay, etc.) is known and constants for the soil type can be estimated by comparing the soil under consideration with similar soils that have been tested previously. (Table Va lists the values of constants for the sands.) Of course, if time and facilities are available, creep tests should be made on the actual soil under consideration to determine both the long-term strength and the total strain for any particular stress.

Table Va. Constants for strain equation.

Material	w	K	a (θ in F deg)	σ_{01} (psi)
Ottawa sand	9	0.76	0.98	15,000
Manchester fine sand	35	0.71	0.46	16,400

Table Vb. Comparison of constants for strain equations.

Material	a	K	k	m	a/K	k/m
Ottawa sand	0.58	0.76	0.97	0.78	0.76	1.24
Manchester fine sand	0.46	0.71	0.97	0.38	0.65	2.55

A temperature dependency comparison can be made between Vialov's modified strain equation,

$$\epsilon_V = \left[\frac{\sigma t \lambda}{w \theta_0^k (\frac{\theta}{\theta_0} + 1)^k} \right]^{1/m} + \epsilon_0 \quad (1)$$

and the strain rate equation,

$$\epsilon_S = \left[\frac{\sigma}{\sigma_{01} \theta_0^a (\frac{\theta}{\theta_0} + 1)^a} \right]^{1/K} \frac{t\psi}{\psi} + \epsilon_0 \quad (2b)$$

By neglecting ϵ_0 and considering strain to be a function of temperature only, the strain functions become:

CREEP OF FROZEN SANDS

$$f_v(\theta) = [\theta_0 \left(\frac{\theta}{\theta_0} + 1 \right)]^{k/n}$$

$$f_s(\theta) = [\theta_0 \left(\frac{\theta}{\theta_0} + 1 \right)]^{a/K}$$

and for $\theta_0 = 1^\circ$ in the same system of units;

$$f_v(\theta) = (\theta + 1)^{k/m}$$

$$f_s(\theta) = (\theta + 1)^{a/K}$$

which indicate that the exponent a/K should be equal to k/m . By using values given in Tables IV and Va and by making the comparison shown in Table Vb, it is clear that the exponents are not equal. However, if we substitute test values into both equations, we find that for: Ottawa sand at 15F ($\theta = 17F$) and $\sigma = 170$ psi eq 1 yields

$$\epsilon_v - \epsilon_0 = \left[\frac{170 t^{0.35}}{5,500 (17 + 1)^{0.97}} \right]^{1/0.78} \quad \text{in psi, hr, and F deg.}$$

$$\epsilon_v - \epsilon_0 = 3.3 \times 10^{-4} t^{0.45}$$

and for: $w = 9$, $M = \sigma^1/w = 170^1/9 = 1.77$

$$\psi = \frac{M - 1}{M} = \frac{1.77 - 1}{1.77} = 0.44$$

equation 2b gives

$$\epsilon_s - \epsilon_0 = \left[\frac{170}{15,000 (17 + 1)^{0.58}} \right]^{1/0.76} \frac{t^{0.44}}{0.44} \quad \text{in psi, hr and F deg.}$$

$$\epsilon_s - \epsilon_0 = 6.85 \times 10^{-4} t^{0.44}$$

which shows that equation 1 gives values of about one half of equation 2. Perhaps M is not entirely independent of temperature; this should be investigated further.

Strength - time

Using the time to total failure and the corresponding applied failure stress from the strain vs time curves, curves for strength vs time at different test temperatures were plotted on Figures 39 and 40. The curves are drawn to approach asymptotically the value of the maximum applied test stresses that did not cause failure during the test period (i.e., a stress known to be less than the long-term strength). At the termination of each test in which the specimen did not fail, the measured rate of strain was either zero (i.e., no deformation change could be detected for at least 100 hours), or the rate of deformation was decreasing continuously after a total test period of over 2000 hours. The curves and test data in Table VI show that the saturated frozen sands have long-term strengths of less than 15% of their instantaneous strength. It should be noted on Figures 39 and 40 that ice strengths are less than those of the sands tested under the same conditions.

Vialov (1959) suggests that the variation of strength of frozen soils with time is an exponential function in the form

$$\sigma_{ult} = \frac{\beta}{\ln(t/B)} \quad (7)$$

where β and B are parameters which depend upon the soil and its temperature and t and σ_{ult} are the time to either failure or incipient failure, and failure stress, respectively. For convenience in graphic plotting, the logarithm to the base ten is used to evaluate β and B ; then eq 7 becomes:

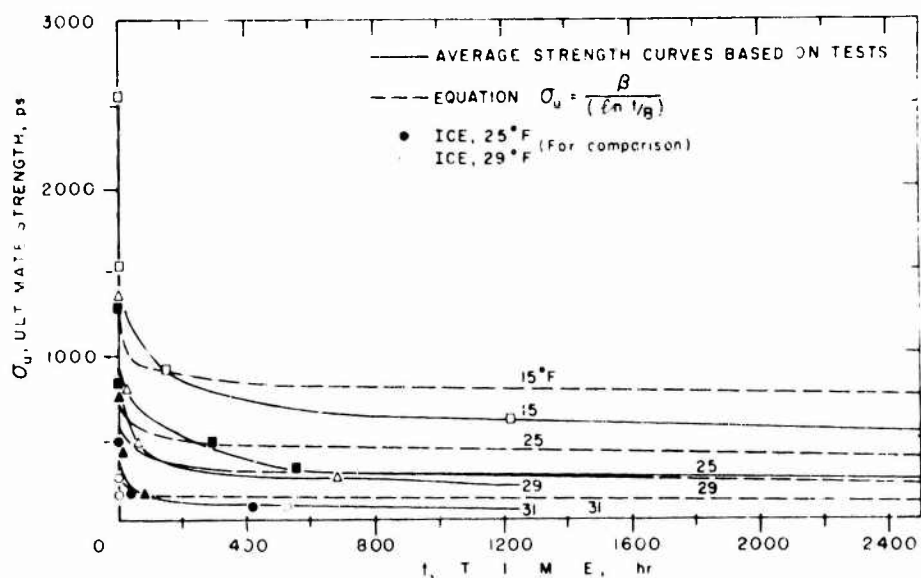


Figure 39. Ultimate strength and time to failure, Ottawa sand (20-70).

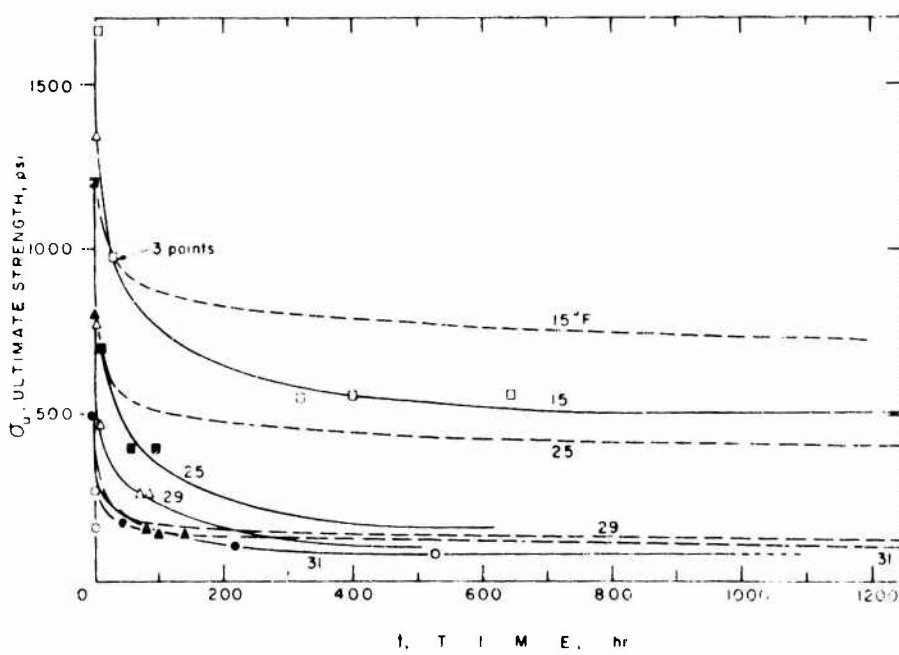


Figure 40. Ultimate strength and time to failure, Manchester fine sand.

CREEP OF FROZEN SANDS

Table VI. Long-term unconfined compressive strength.

Temp (°F)	Instantaneous strength (psi)	Predicted long-term strength (psi)		Creep test stress	
		I*	II†	Non-failure (psi)	Failure (psi)
15	2530	420	572	170	600
24.5	1460	254	263	200	460
29	1320	134	149	100	250
31	745	69	76	40	80

Manchester Fine Sand					
15	2790	329	343	350	560
25	2000	176	193	160	400
29	1340	115	128	100	265
31	805	63	66	80	150

* I - predicted long-term strengths are for 100 years determined by eq 7a using Figures 41 and 42 to determine values for B and β . See Table VII.

† II - predicted long-term strengths are the 100-year strength determined by eq 7a using two short-term creep strength values (e.g., 60 and 35% of instantaneous strength) to evaluate B and β .

Table VII. Constants for eq 7a as determined from Figures 41 and 42.

Temp (°F)	Ottawa Sand		Manchester Fine Sand	
	B (hr)	β (psi)	B (hr)	β (psi)
15	0.0031	3590	0.0126	2600
25	0.0189	1960	0.0424	1290
29	0.1	1000	0.0394	852
31	0.0994	475	193	420

$$\sigma_{ult} = \frac{\beta}{\log(t/B)} \quad (7a)$$

The values of parameters β and B can be determined by either developing a plot of $1/\sigma_{ult}$ vs time or by using results from short-term creep tests. Figures 41 and 42 indicate Vialov's method of determining these parameters from the $1/\sigma_{ult}$ vs log time curves. These curves are based on results of both short-term and long-term creep tests and can be used to predict failure strengths more accurately than by using only short-term creep test results alone. The disadvantage of using these plots is the length of time and care required to perform the long-term creep tests. Using the results of short-term creep tests for predicting long-term strength has the advantage of requiring only two simple creep tests that can be performed at two different stress levels within a period of 3 days. Values of β and B can be determined by solving eq 7a using the results of these two tests. For comparison, values of the 100-year predicted strengths are shown in Table VI in columns I and II as determined by the $1/\sigma_{ult}$ vs log time curves and by two short-term creep tests, respectively.

CREEP OF FROZEN SANDS

41

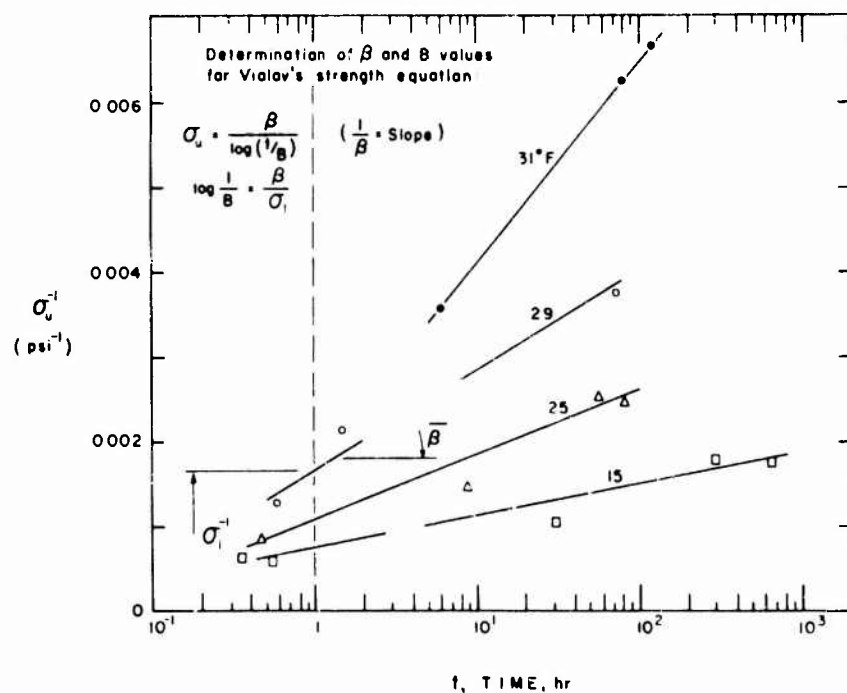


Figure 41. Time and reciprocal of ultimate stress, Manchester fine sand.

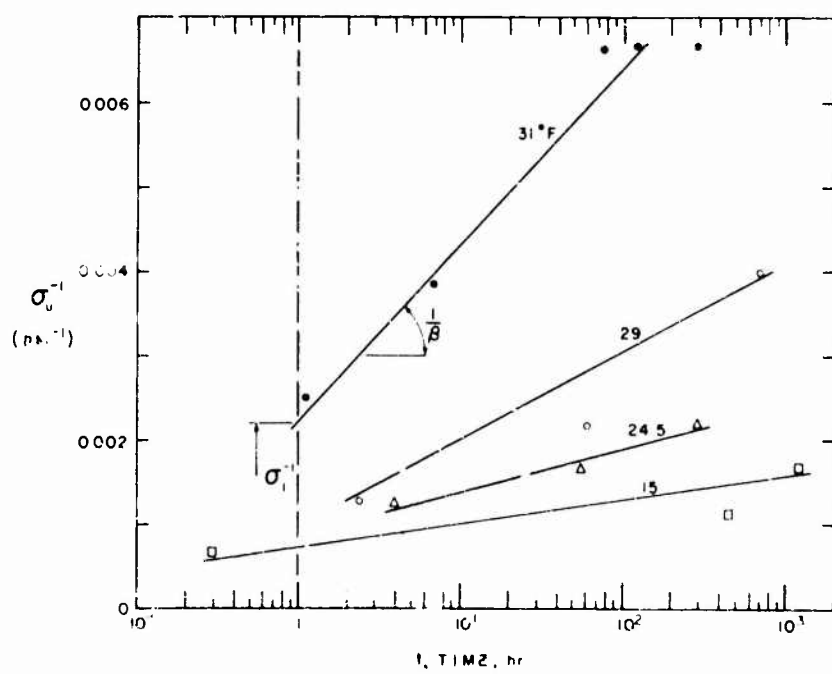


Figure 42. Time and reciprocal of ultimate stress, Ottawa sand (20-30).

CREEP OF FROZEN SANDS

It should be noted that Vialov's strength equation (eq 7) should not be used for extremely short periods, since when the duration of loading approaches zero it predicts strengths approaching infinity. This restriction does not invalidate the equation's usefulness in predicting the long-term strength of the frozen soil.

Further examination of Table VI shows that, with the exception of Manchester fine sand at 15 and 31°F, the predicted long-term strength for both soils at the different temperatures is greater than the tested long-term strength (non-failure value in the table) and less than the next higher test stress level that caused failure. Strength variations with time predicted by eq 7a using two short-term creep tests are compared with test strength values in Figures 39 and 40. The figures and Table VI show that the Vialov equation may predict unsafe strength values if based on short-term creep parameters unless an appropriate factor of safety is used.

An examination of Figures 39 and 40 reveals that the greatest loss of strength for frozen sand occurs during a relatively short period after application of stress. By comparing values in Table VIII, it is clear that the ability of the frozen sand to resist complete failure is reduced by at least 50% of its instantaneous strength when the applied stress acts 24 hours and that further strength reductions occur at a much lower rate. Also, stresses that are to be resisted for 1000 hours must be reduced to less than 25% of the instantaneous strength of the frozen sand. It should be emphasized that percentages shown in Table VIII are to demonstrate the strength reduction of frozen sand and are based on an "instantaneous" strength defined in this report.

Table VIII. Percent of instantaneous strength loss after application of stress.

Ottawa Sand (20-30)

Time after stress application

Temp °F	1 hr	24 hr	100 hr	1000 hr
15	45	55	60	75
25	25	50	55	80
29	25	50	70	80
31	45	70	80	90

Manchester Fine Sand

15	45	65	70	80
25	45	70	80	90
29	55	75	80	95
31	50	70	80	90

Strength - temperature

Except for the instantaneous strength curve, the strength vs temperature curves on Figures 43 and 44 are replotted from the strength vs time curves for the various times of stress application shown. The instantaneous strength curves are drawn through the average instantaneous strength points and for comparison purposes instantaneous ice strengths are plotted on the figures. The long-term strength curves are based on extrapolations of the strength vs time curves.

CREEP OF FROZEN SANDS

43

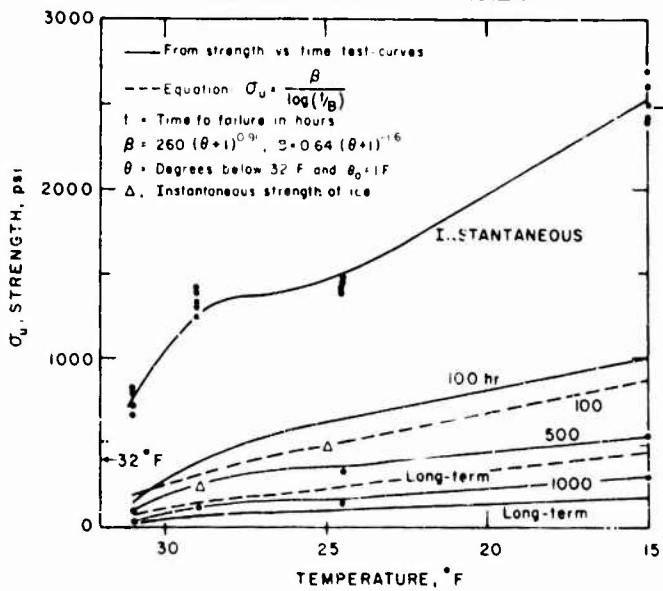


Figure 43. Strength for various conditions, Ottawa sand (20-30).

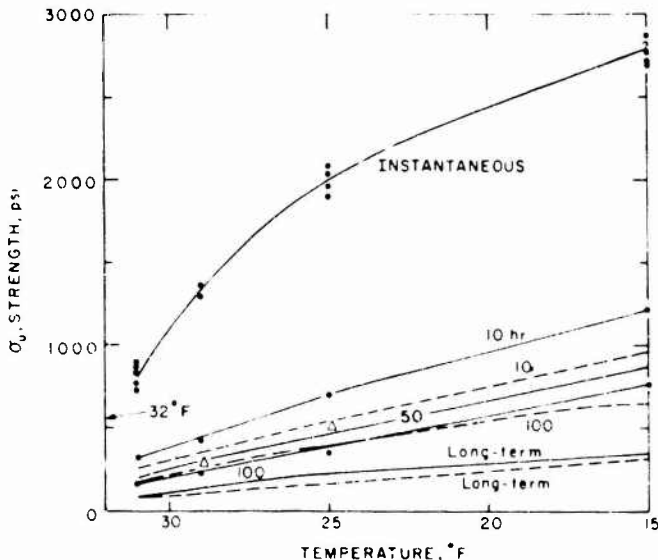
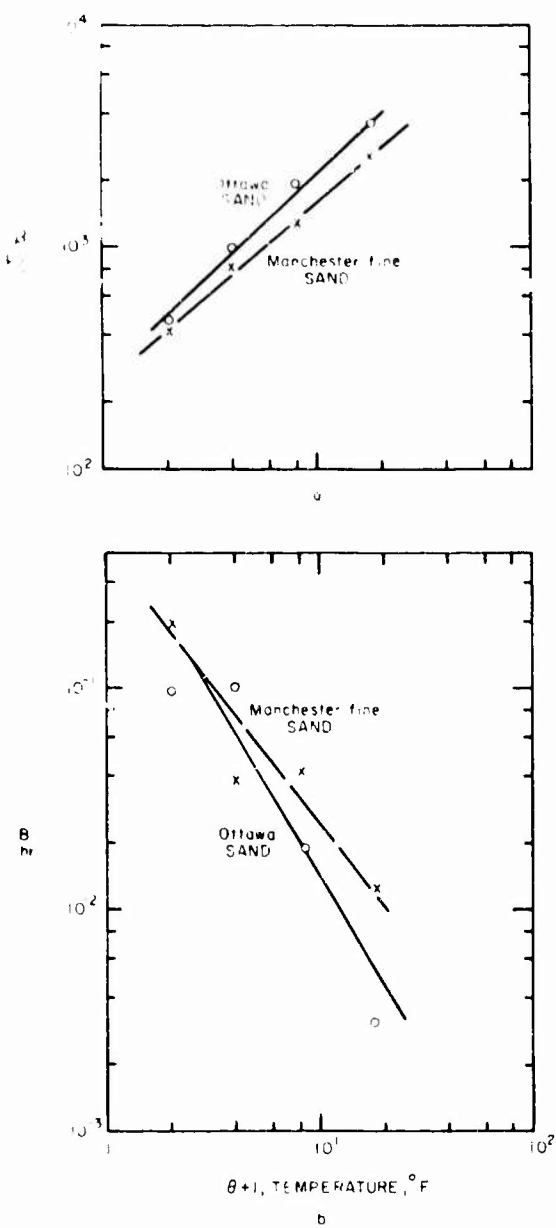


Figure 44. Strength for various conditions, Manchester fine sand.

In Figure 43, the instantaneous strength curve for Ottawa sand shows unexpected change in strength values near 29°F. A similar change in strength in this temperature range has been observed by others (ACFEL, 1952). It was noted that at 25°F and 15°F brittle types of failures occurred and at 31°F all failures were plastic. One possible explanation for strength irregularity is that a transition between brittle and plastic type failure occurs at about 29°F. The type of specimen failure for a constant temperature depends upon both density and rate of loading. The influence of specimen density is suggested by comparing strength vs temperature curves for Manchester fine sand reported by ACFEL (1952) with the instantaneous strength curve on Figure 44. The ACFEL tests performed on

CREEP OF FROZEN SANDS

Figure 45. Temperature, β and B parameters.

$$\theta_0 = 1 \text{ F}$$

specimens with void ratios of 0.658 show an irregular strength curve near 25°F while the tests shown on Figure 44 (average void ratios of 0.78) did not reveal this irregularity even though the rate of loading was over five times greater than that applied by ACFEL. Also, all specimens reported on Figure 44 failed plastically. A further investigation of instantaneous strength is required for a positive explanation of the results shown in this report.

The curves in Figures 43 and 44 show that frozen sand strength increases with decreasing temperatures and that the increase in long-term strength is less for a given temperature reduction than the short-term strength increase. For example, Ottawa sand showed an instantaneous strength increase of 2000 psi while the long-term strength increased only 150 psi for a temperature decrease from 31°F to 15°F.

For the temperature range tested, the long-term strength increase with decreasing temperature may be approximated by the equation $\sigma_{ult} = a + b|\theta|^n$ (suggested by Vialov, 1959) where n , a and b are constants. b has the units of stress/degrees n .

The long-term strength of Ottawa sand may be represented by:

$$\sigma_{ult} = 20|\theta|^{3/4} \text{ in psi and F deg}$$

and similarly that for Manchester fine sand may be expressed by:

$$\sigma_{ult} = 40 + 40|\theta|^{3/4} \text{ in psi and F deg.}$$

Figures 41 and 42 and Table VII show that β and B are functions of temperature. Plots in logarithmic coordinates of β and B vs a temperature function are shown in Figures 45a and b. Equations for the straight lines approximating the plotted data for Ottawa sand are:

$$\beta = 260\theta_0^{0.91}(1 + \frac{\theta}{\theta_0})^{0.91}$$

$$B = 0.64\theta_0^{-1.6}(1 + \frac{\theta}{\theta_0})^{-1.6}$$

For $\theta_0 = 1F$

$$\beta = 260(1 + \theta)^{0.91}$$

$$B = 0.64(1 + \theta)^{-1.6}$$

and for Manchester fine sand:

$$\beta = 240\theta_0^{0.82}(1 + \theta)^{0.82}$$

$$B = 0.43\theta_0^{-1.24}(1 + \theta)^{-1.24}$$

For $\theta_0 = 1F$

$$\beta = 240(1 + \theta)^{0.82}$$

$$B = 0.43(1 + \theta)^{-1.24}$$

where β is in psi, B is in hours and θ in F deg.

By substituting computed values for β and B in eq 7a, strength values for various temperatures and periods of stress application can be computed. Computed strength values plotted on Figures 43 and 44 are in good agreement with the data curves shown on the same figures.

The increase in strength of frozen soil as the temperature decreases is generally attributed to the reduction of the amount of unfrozen water in the soil and to increased strength of the pore ice. Since the amount of unfrozen water in sand is extremely small and its influence on strength may be neglected, then the main factor affecting change in strength with temperature is the pore ice. Tests performed by Butkovich (1954) on lake ice and on commercially frozen ice showed a marked increase in strength with a decrease in temperature which is in agreement with the increase in strength noted in saturated frozen sands.

CONCLUSIONS

The primary factors affecting the strength and deformation of a given saturated frozen sand under static load are temperature and duration of stress. (Density is another important factor, however it was not investigated in this report.) The results of this investigation which are based on unconfined compression tests performed on saturated frozen Ottawa sand and Manchester fine sand show that:

a. Long-term strength is less than 15% of instantaneous strength. Vierow's strength equation, $\sigma_{ult} = \frac{\beta}{\ln(t/B)}$ [or $\sigma_{ult} = \beta/\log(t/B)$], can be used to predict creep strengths of saturated frozen sand based on short-term creep parameters provided that a factor of safety of 1.5 to 2 is used. For the density and test conditions the parameters β and B can be considered to be functions of temperature determined approximately for frozen saturated Ottawa sand by:

$$\beta = 260 \theta_0^{0.91} \left(1 + \frac{\theta}{\theta_0}\right)^{0.91}$$

$$B = 0.64 \theta_0^{-1.6} \left(1 + \frac{\theta}{\theta_0}\right)^{-1.6}$$

and for Manchester fine sand by:

$$\beta = 240 \theta_0^{0.82} \left(1 + \frac{\theta}{\theta_0}\right)^{0.82}$$

$$B = 0.43 \theta_0^{-1.24} \left(1 + \frac{\theta}{\theta_0}\right)^{-1.24}$$

where β is in psi, B is in hours, θ is Fahrenheit degrees below 32F and θ_0 is a reference temperature, >0, F deg.

b. As the temperature decreases, strength increases. The long-term strength of frozen saturated Ottawa sand can be represented approximately by

$$\sigma_{ult} = 20 |\theta|^{3/4}$$

where σ_{ult} is in psi and θ is in F deg [the strength at 32F ($\theta=0$) is very small and extremely difficult to obtain; extrapolation is doubtful, so zero strength is assumed]; and Manchester fine sand by:

$$\sigma_{ult} = 40 + 40 |\theta|^{3/4}$$

c. Deformation increases with increased stress, time and temperature. Unconfined compression strains can be predicted by:

$$(1) \quad \epsilon = \left[\frac{\sigma}{\sigma_0 \theta_0^a \left(\frac{\theta}{\theta_0} + 1 \right)^a} \right]^{1/K} \cdot \frac{t \psi}{\psi} + \epsilon_0$$

where: σ = applied constant stress

t = time

ψ = $(M-1)/M$

M = $\sigma t / w$

θ = °F below 32F

θ_0 = reference value of θ , F deg

and the constants σ_0 , K , a and w are listed in Table V.

(2) Vialov's equation

$$\epsilon = \left[\frac{\sigma t^\lambda}{\omega \theta_0^k (\frac{\theta}{\theta_0} + 1)^k} \right]^{1/m} + \epsilon_0$$

where the constants m, λ , ω and k are listed in Table IV.

d. For a constant temperature and an applied constant stress the strain can be predicted approximately by:

$$\epsilon = \epsilon_1 \cdot \frac{t^\psi}{\psi}$$

where: $\psi = \frac{M-1}{M}$ and M and ϵ_1 can be determined graphically by a creep test lasting only 8 hours. Further research is desirable to investigate a possible temperature effect on M.

e. Strains for stresses less than the long-term strength are composed of less than 14% elastic strain (of this less than 7% is instantaneous and 10% time-dependent elastic) and, further, that the irreversible strain is dominant even at this stress level.

f. Unconfined compression creep tests with constant stresses below the long-term strength reveal that the rate of strain is directly proportional to the reciprocal of time during stress application until complete stabilization occurs.

This investigation has attempted to relate empirically the effect of temperature and time to both the strength and deformation characteristics of remolded, artificially frozen soils subjected to uniaxial compression. The effect of density of the frozen soil, the soil particle characteristics (i.e., size, shape, mineral composition, etc.), the water content (both frozen and unfrozen), and the influence of a more complex state of stress are items that still remain for future experimental investigations. A practical theory that will permit a better utilization of laboratory and field test results in the design of engineering structures in frozen soil must still be developed before the real potential of frozen soil as an engineering material can be realized. Therefore, the present investigation can be viewed only as an extension of the initial step taken by ACFEL (1952) toward a practical solution of engineering problems in permanently frozen soil.

LITERATURE CITED

- Assur, A. (1963) Creep of frozen soil (Discussion), Proceedings of the First International Conference on Permafrost, Building Research Advisory Board, National Academy of Sciences, p. 339.
- Arctic Construction and Frost Effects Laboratory (1952) Investigation of description, classification and strength properties of frozen soils, U.S. Army Corps of Engineers, New England Division, ACFEL TR 40. (Also U.S. Army Snow, Ice and Permafrost Research Establishment (USA SIPRE) Report 8.)
- Butkovich, T.R. (1954) Ultimate strength of ice. USA SIPRE Research Report 11.
- and Landauer, J. K. (1959) The flow law for ice, USA SIPRE Research Report 56.
- (1960) Creep of ice at low stresses, USA SIPRE Research Report 72.

LITERATURE CITED (Cont'd)

- Glen, J. W. (1955) The creep of polycrystalline ice, Proceedings of the Royal Society (London), Ser. A, vol. 228, p. 519-538.
- Jellinek, H. H. G. and Brill, R. (1956) Viscoelastic properties of ice, Applied Physics, vol. 27, no. 10, p. 1198-1209.
- Sanger, F. J. and Kaylor, C. W. (1963) Plastic deformation of frozen soils in unconfined compression, Proceedings of the First International Conference on Permafrost, Building Research Advisory Board, National Academy of Sciences.
- Tsytovich, N. A. (1954) Instructions for determining the forces of adhesion of frozen soil, U.S. Army Cold Regions Research and Engineering Laboratory (USA CRREL) Draft Translation.
- (1958) Bases and foundations on frozen soil, Academy of Sciences, USSR. Highway Research Board Translation, Special Report 58, 1960.
- Vialov, S. S. (1959) Rheological properties and bearing capacity of frozen soils, Academy of Sciences, USSR. USA CRREL Translation 74, 1965.
- (Editor) (1962) Strength and creep of frozen soils and calculations for ice-soil retaining structures, Academy of Sciences, USSR. USA CRREL Translation 76, 1965.
- and Tsytovich, N. A. (1955) Cohesion of frozen soils, Dok. Akad. Nauk. 104, vol. 4, p. 527-529.

APPENDIX A: SPECIMEN PHYSICAL DATA

49

Table A1. Ottawa sand (20-30).

Specimen No.	f_d lb/in. ³	l_m lb/in. ³	V_1 $\bar{\text{V}}_S$	s_1	Stress lb/in. ²	% of voids	Time to fail	Plastic flow (P.F.)	Failure strain	Remarks
<u>Nominal temp 15°F</u>										
OWS-67	104.5	125.6	.593	.98.6	601	0.375	2.694*	106.5	1.5	6.2"
OWS-69	105.1	125.7	.575	.97.1	.592	0.372	2.612*	103.2	1.5	9.2"
OWS-70	104.9	126.0	.586	.98.7	.593	0.372	2.410*	95.3	1.5	8.9"
OWS-74	104.6	125.8	.591	.98.8	.600	0.375	2.428*	98.0	1.5	7.5"
OWS-76	105.5	126.4	.578	.98.8	.584	0.369	2.503*	98.9	1.5	5..
OWS-62	104.8	126.0	.591	.99.0	.596	0.374	1.497	59.4	1.5	6.30"
OWS-63	104.8	125.9	.588	.98.6	.596	0.373	1.494	59.1	1.5	25.50"
OWS-64	104.4	125.6	.600	.99.2	.605	0.377	1.500	59.3	1.5	10' 15"
OWS-66	104.8	126.5	.588	.98.9	.596	0.373	1.496	59.1	1.5	35..
OWS-71	104.7	125.7	.584	.98.3	.594	0.373	1.888	35.1	1.5	46 hr
OWS-73	104.8	125.6	.589	.98.7	.596	0.373	1.886	35.0	1.5	165 hr
OWS-75	105.1	126.1	.585	.98.3	.591	0.372	1.891	35.2	1.5	93 hr F
OWS-77	105.1	125.9	-	-	-	-	-	140 hr	83 hr	0.084
OWS-79	104.7	125.9	.586	.98.8	.593	0.373	1.883	34.9	1.5	120 hr F
OWS-80V	105.	125.9	.588	.98.	.600	0.370	1.870	33.7	1.5	1130 hr
OWS-80V	105.4	126.2	.578	.98.4	.586	0.370	1.866	23.7	1.5	645 hr
OWS-60	102.3	123.9	.619	.97.1	.637	0.390	1.860	23.7	1.5	1300 hr
OWS-68	104.0	125.3	.597	.98.2	.607	0.378	1.770	6.7	1.5	690 hr
OWS-72	105.0	126.3	.585	.98.7	.593	0.372	1.770	6.7	1.5	1469 hr
OWS-78	104.5	125.6	.590	.98.2	.600	0.375	1.770	6.7	1.5	1468 hr
<u>Average instantaneous strength = 2530 psi</u>										
<u>Nominal temp 25°F</u>										
OWS-130	104.1	125.6	.603	.99.4	.606	0.377	1.447*	99.04	24.5	7.2"
OWS-158	106.3	126.6	.558	.97.3	.572	0.364	1.471*	100.68	24.5	11.2"
OWS-164	105.9	126.5	.567	.97.9	.579	0.365	1.491*	102.05	24.5	14.1"
OWS-166	106.2	126.2	.565	.98.2	.575	0.365	1.449*	99.18	24.5	11.2"
OWS-171	106.6	126.9	.558	.98.5	.566	0.360	1.446*	98.97	24.5	10.0"
OWS-53	104.1	125.2	.592	.99.6	.594	0.378	1.790	54.1	24.5	277.0"
O'S-56b	104.5	125.6	.588	.98.1	.599	0.375	1.789	54.0	24.5	277.0"
OWS-30V	105.1	125.6	.598	.591	.591	0.371	1.600	41.1	24.5	51 hr
OWS-43V	104.2	125.5	.596	.98.5	.605	0.377	1.460	31.5	24.5	263 hr
OWS-46V	104.4	125.8	.591	.98.9	.598	0.374	1.460	31.5	24.5	306 hr
OWS-47V	104.5	125.2	-	-	-	-	-	24.5	24.5	506 hr
OWS-23	103.9	125.0	.603	.98.8	.607	0.378	2.00	13.7	24.5	3501 hr F
OWS-31V	104.0	125.2	.596	.97.9	.608	0.378	2.00	13.7	24.5	3090 hr F
OWS-32V	105.2	126.0	.561	.97.4	.576	0.370	2.00	13.7	24.5	197 hr F
OWS-18	101.7	121.1	.585	.90.9	.643	0.391	50	3.42	25	Power failure
OWS-18a	102.4	122.1	.591	.94.5	.624	0.384	50	3.42	25	Rebounded and power failure
OWS-19	103.6	123.0	.551	.90.2	.611	0.379	50	3.42	25	Power failure
OWS-19a	101.9	123.2	.610	.95.2	.640	0.391	50	3.42	25	Rebounded and power failure
OWS-20	102.5	123.8	.597	.94.4	.635	0.365	50	3.42	25	Rebounded and power failure
OWS-20a	101.7	122.5	.610	.94.7	.644	0.341	50	3.42	25	Rebounded and power failure
<u>Average instantaneous strength = 1460 psi</u>										
f_d	Dry unit wt	V_1	Void ratio	V_1	Max. stress	P.F.	Point on time-strain curve where plastic flow begins			
in.	Mass unit wt	Vol. of ice	*	VS	Duration of test	F				
	Vol. of soil grains	$\bar{\text{V}}_S$		S ₁	Tests performed on constant stress apparatus	V				

APPENDIX A

Table A1. (Cont'd)

Specimen No.	r_d lb/ft ³	r_m lb/ft ³	$\frac{V_I}{V_S}$	S_I	e	Porosity	Stress lb/in. ²	% of area Inst.	Nominal temp. 29°F	Plastic flow (P.F.)			Failure strain	Remarks
										Time to fail	Temp. °F	Time strain		
OWS-92	104.1	125.4	.598	.93.7	0.606	0.377	1197	90.6	29	41.3'	-	-	-	0.00337
OWS-93	104.2	125.0	.570	.99.1	0.575	0.359	1409	106.7	29	7.3'	-	-	-	0.00226
OWS-96	104.4	125.4	.589	.97.7	0.602	0.376	1250	94.6	29	7.0'	-	-	-	0.00246
OWS-98	103.9	125.0	-	-	-	-	1394	105.5	29	7.2'	-	-	-	0.00246
OWS-83	104.3	125.5	.594	.98.4	0.603	0.376	1290	97.6	29	6.8'	-	-	-	0.00375
OWS-92	104.3	125.5	.594	.98.5	0.603	0.376	1325	100.3	29	6.8'	-	-	-	0.00380
OWS-119	104.5	125.7	.591	.98.5	0.599	0.375	1306	98.9	29	8.0'	-	-	-	0.00312
OWS-123	104.3	125.2	.596	.98.8	0.603	0.376	1386	104.9	29	7.3'	-	-	-	0.00246
OWS-86	103.8	125.0	.597	.97.7	0.609	0.379	1775	58.7	29	3 hr 59'	-	-	-	0.00246
OWS-146	105.0	126.0	.586	.98.6	0.593	0.372	1223	92.6	29	6.9'	-	-	-	0.00246
OWS-159	106.4	126.75	.560	.97.8	0.572	0.364	1352	102.3	29	8.0'	-	-	-	0.00246
OWS-160	106.1	126.66	.567	.98.3	0.576	0.366	1291	97.7	29	7.0'	-	-	-	0.00246
OWS-165	106.3	126.69	.560	.94.7	0.573	0.364	1399	105.9	29	7.2'	-	-	-	0.00246
OWS-169	106.6	126.61	.547	.96.3	0.568	0.362	1233	99.3	29	6.4'	-	-	-	0.00246
OWS-172	106.4	127.13	.568	.99.1	0.571	0.364	1316	99.6	29	6.6'	-	-	-	0.00246
OWS-84	104.5	125.7	.594	.98.8	0.600	0.375	776	58.7	29	2 hr 48'	-	-	-	0.076
OWS-100	104.3	125.5	.594	.98.4	0.604	0.376	778	58.9	29	59'	36'	0.047	Specimen twisted	0.047
OWS-810	104.9	125.9	.586	.98.6	0.594	0.373	775	58.7	29	2 hr 8'	1 hr	-	-	0.061
OWS-87V	104.2	125.5	.599	.98.8	0.606	0.377	460	34.8	29	40"	35"	0.086	Specimen twisted	0.086
OWS-104V	104.0	125.7	-	-	-	-	460	34.8	29	55 hr	47 hr	0.071	Rebounded	0.071
OWS-107V	104.2	125.5	.599	.99.0	0.605	0.397	460	34.8	29	40 hr	35 hr	0.074	Rebounded	0.074
OWS-111V	104.4	125.7	.597	.99.1	0.602	0.376	460	34.8	29	53 hr	415 hr	0.071	Rebounded	0.071
OWS-118V	104.2	125.5	.595	.98.4	0.604	0.377	250	18.9	29	849 hr	532 hr	0.060	Rebounded	0.060
OWS-88V	104.5	125.7	.591	.98.6	0.599	0.375	250	18.9	29	1080.5 hr F	-	-	-	1080.5 hr F
OWS-99	104.6	125.7	.590	.98.5	0.599	0.375	100	7.6	29	1244 hr F	-	-	-	1244 hr F
OWS-94	104.6	125.7	.591	.98.6	0.599	0.375	100	7.6	29	1244 hr F	-	-	-	1244 hr F
OWS-88	106.8	125.4	.511	.98.9	0.516	0.339	100	7.6	29	1243 hr F	-	-	-	1243 hr F
OWS-37	104.7	125.7	.507	.98.2	0.597	0.374	100	7.6	29	1243 hr F	-	-	-	1243 hr F

Average instantaneous strength = 1320 psi.

 r_d = Dry unit wt r_m = Mass unit wt V_I = Vol. of ice $\frac{V_I}{V_S}$ = Vol. of soil grains S_I = Percent of voids filled with ice e = Void ratio

P.F. = Point on time-strain curve where plastic flow begins

Max. stress

Duration of test

Tests performed on constant stress apparatus

APPENDIX A

Table A1. (Cont'd)

Specimen No.	γ_d lb/ft ³	f_m lb/ft ²	V_1	S_1	ϵ	Porosity	Nominal temp 31°F	Stress lb/in. ²	% of Inst. Strength	Temp °F	Time to fail	Plastic flow (P.F.)	Failure strain	Remarks
OWS-114	103.5	125.1	.611	99.1	0.616	.381	744.3	99.9	31	10.6*				0.00247
OWS-110	103.6	125.0	.603	98.3	0.613	.381	683.9	91.8	31	6.8*				0.00243
OWS-105	104.4	125.6	.594	98.6	0.602	.375	784.4	105.3	31	6.8*				0.00240
OWS-117	104.4	125.6	.593	98.4	0.603	.376	767.1	103.0	31	6.8*				0.00272
OWS-116V	103.5	125.0	.606	98.3	0.616	.381	400	53.7	31	30*				0.015
OWS-101V	104.6	125.7	.588	98.3	0.598	.376	400	53.7	31	2 hr 30*	1 hr			0.040
OWS-102V	104.5	125.6	.589	98.2	0.600	.375	400	53.7	31	10*				-
OWS-136V	104.8	125.9	.587	98.5	0.596	.373	260	34.9	31	6 hr 30*				0.01
OWS-138V	105.2	126.1	.580	98.4	0.589	.371	260	34.9	31	6 hr	1 hr			0.02
OWS-152V	105.1	126.1	.582	98.5	0.591	.371	260	34.9	31	6 hr	2 hr			0.02
OWS-152V	105.9	126.5	.568	98.1	0.579	.367	150	20.1	31	9 hr	3.5 hr			0.023
OWS-139V	104.5	125.8	.596	99.2	0.600	.375	150	20.1	31	53 hr F	-			Cold room breakdown (~4 hr)
OWS-134V	104.9	125.9	.585	99.3	0.589	.373	150	20.1	31	72 hr	53 hr			0.047
OWS-149V	105.4	126.2	.576	97.4	0.591	.371	150	20.1	31	78 hr 59*	60 hr			0.048
OWS-150V	105.2	126.1	.578	98.1	0.589	.371	150	20.1	31	120 hr	120 hr			0.049
OWS-151V	105.5	126.3	.577	98.5	0.585	.369	150	20.1	31	288 hr	146 hr F			Ends restrained and wt on REST
OWS-12:	103.7	125.1	.603	98.4	0.612	.380	80	10.7	31	6 hr F	-			Specimen twisted
OWS-122	104.3	125.5	.592	98.1	0.603	.376	80	10.7	31	7 hr F	-			Gage slipped
OWS-125	102.8	125.9	.623	99.7	0.624	.385	80	10.7	31	94 hr F	-			Temp rise ~ cabinet failure
OWS-124	104.7	125.8	.588	98.6	0.596	.374	40	5.4	31	542 hr F	-			Cold room breakdown
OWS-120	103.7	125.1	.603	97.9	0.615	.382	40	5.4	31	144 hr F	-			Gage slipped
OWS-137	104.5	125.8	.592	98.5	0.601	.375	40	5.4	31	240 hr F	-			Cold room breakdown
OWS-145	104.1	125.4	.599	98.8	0.606	.378	40	5.4	31	168 hr F	-			Cold room breakdown
OWS-132	104.6	125.8									2.7	31		
OWS-143	105.2	126.3									2.7	31		
OWS-140	104.7	125.9									2.7	31		
Average instantaneous strength = 745 psi														

γ_d = Dry unit wt
 γ_m = Mass unit wt
 V_1 = Vol. of ice
 \bar{V}_S = Vol. of soil grains
 S_1 = Percent of voids filled with ice

e = Void ratio
 ϵ = Point on time-strain curve where plastic flow begins
 σ = Max. stress
 Δ = Duration of test
 F = Tests performed on constant stress apparatus

P.F. = Point on time-strain curve where plastic flow begins
 F = Duration of test
 V = Tests performed on constant stress apparatus

APPENDIX A

Table AII. Manchester fine sand.

Specimen No.	r_d lb./ft. ³	r_m lb./ft. ³	v_i v_s	s_i	e	Porosity	Stress lb./in. ²	% of Inst. Strength	Temp. °F	Time to fail	Plastic flow (P.F.)	Failure strain	Remarks
Nominal temp 15°F													
A VS 54	95.3	120.35	.769	99.8	.770	.435	2750	98.67	15	13.9"	-	.01201	Recorder failure
63	96.4	120.60	.743	98.4	.754	.430	2774	99.53	15	-	-	.01038	
76	95.3	119.86	.763	98.4	.775	.437	2962	102.69	15	14.5"	-	.00994	
77	95.3	119.87	.762	98.3	.774	.436	2811	100.86	15	13.8"	-	.01116	
82	94.9	119.68	.771	98.6	.782	.439	2736	98.17	15	14.2"	-		
85	95.5	120.09	.760	98.7	.770	.435	1659	60.0	15	17.4*	12"	.188	
87	95.1	120.08	.776	99.7	.778	.438	1659	60.0	15	17.4*	22"	.221	
94	94.5	119.48	.783	99.0	.750	.441	1663	59.7	15	13.3"	13"	.165	
95	95.8	120.30	.755	98.7	.765	.433	1661	59.6	15	32.8*	14"	.151	
84	-	119.86	-	-	-	-	979	34.98	15	23 hr	10.5 hr	.250	Error in weighing
89	94.46	120.16	.765	99.1	.771	.435	975	34.98	15	26 hr	9.5 hr	.203	
92	95.38	120.08	.765	98.9	.773	.436	975	34.98	15	30 hr	10 hr	.198	
75V	94.6	119.62	.780	99.1	.786	.440	560	20.09	15	645 hr	380 hr	.130	
78V	93.8	119.08	.796	99.1	.803	.445	560	20.09	15	400 hr	180 hr	.127	
88V	94.8	119.30	.762	97.4	.782	.439	560	20.09	15	320 hr	160 hr	.150	Error in weighing
72V	96.81	120.33	-	-	-	-	350	12.56	600 hr	F	-	-	Error in weighing
91V	96.86	120.28	-	-	-	-	350	12.56	696 hr	F	-	-	Error in weighing
80	95.7	120.23	.756	98.6	.766	.434	200	7.18	793 hr	F	-	-	
81	94.3	119.30	.782	98.7	.792	.442	200	7.18	793 hr	F	-	-	
79	93.6	118.82	.794	98.5	.805	.446	150	5.38	793 hr	F	-	-	
90	94.2	119.12	.782	98.3	.798	.443	150	5.38	793 hr	F	-	-	
Average instantaneous strength = 2790 psi													
Nominal temp 25°F													
27	95.60	120.10	.758	98.5	.769	.435	1973*	98.7	25	13.3"	-	.01743	L. M. P. failure
57	95.55	120.13	.760	98.7	.770	.434	1901*	95.1	25	12.5"	-	.01381	
60	95.66	120.21	.756	99.2	.761	.432	2040*	102.1	25	11.7"	-	.01198	
65	94.93	119.86	.797	98.8	.807	.439	2083	104.2	25	14.7"	-		
50	95.58	120.13	.759	98.6	.769	.435	1198	59.9	25	29.30"	0.25	.0.23	
64	95.94	120.16	.761	98.9	.769	.435	1199	60.0	25	23.36"	0.20	.0.24	
68	95.86	120.36	.754	98.7	.763	.433	1199	60.0	25	29	0.30	.0.24	
51	95.46	120.04	.761	98.6	.771	.435	694	34.7	25	8.5 hr	F	4.42	0.24
52	95.33	119.99	.765	98.8	.774	.436	694	34.7	25	9.1 hr	F	5.0	0.24
53	95.75	120.06	.754	98.7	.767	.434	695	34.8	25	8.15 hr	F	4.70	0.225
55	94.20	119.17	.783	98.5	.795	.443	400	20.0	25	81 hr	52.5 hr	0.18	
58	94.26	119.20	.782	98.4	.794	.441	400	20.0	25	56 hr	35.0 hr	0.15	
67	95.48	120.05	.760	98.5	.771	.435	400	20.0	25	75 hr	47.6 hr	0.15	
69	95.81	120.29	.755	98.7	.765	.433	160	8.0	25	263 hr	F	-	
70	95.30	119.88	.703	93.4	.775	.436	160	8.0	25	365.75 hr	F	-	
Average instantaneous strength = 2000 psi													

r_d = Dry unit wt
 r_m = Mass unit wt
 v_i = Vol. of ice
 v_s = Vol. of soil grains
 s_i = Percent of voids filled with ice

e = Void ratio
 $P.F.$ = Point on time-strain curve where plastic flow begins
 $* =$ Max. stress
 F = Duration of test
 V = Tests performed on constant stress apparatus

APPENDIX A

53

Table AII. (Con'd)

Specimen No.	y_d lb/ft ³	y_m lb/ft ³	$\frac{V_1}{V_S}$	S_1	ϵ	Porosity	Stress lb/in. ²	% of Inst. Strength	Temp °F	Time to fail	Plastic flow (P.F.)	Failure strain	Remarks
<u>Nominal temp 29°F</u>													
3	94.91	119.65	.770	98.5	.781	.439	1327*	98.8	29	11.6"	-	0.0164	
6	95.59	119.58	.781	98.9	.785	.571	1360*	101.3	29	11.9"	-	0.0154	
7	95.05	119.72	.767	98.4	.719	.438	1348*	100.4	29	11.5"	-	0.0154	
11	94.79	119.64	.774	98.6	.783	.440	1336*	99.5	29	11.4"	-	0.0152	
14	94.73	119.60	.776	98.8	.785	.440	771	57.4	29	0.52 hr	0.32	0.26	
19	94.10	120.05	-	-	-	-	770	57.3	29	0.53 hr	0.30	0.26	
23	95.05	119.77	.768	98.6	.779	.433	773	57.6	29	0.62 hr	0.35	0.28	
25	95.64	120.18	.758	98.7	.768	.434	470	35.0	29	5 hr	2.50	0.18	
35	95.15	119.89	.768	98.8	.777	.437	470	35.0	29	3.5 hr	-	-	
40	93.29	119.16	.791	99.0	.799	.444	470	46.7 hr	2.50	4.67 hr	2.50	0.20	
29	95.72	120.19	.755	98.5	.766	.434	265	19.7	29	74.16 hr	30.0	0.12	
61	95.88	120.31	.753	98.6	.763	.433	265	19.7	29	71.84 hr	32.5	0.15	
30	94.2	119.31	.786	98.9	.794	.443	100	7.4	29	59.9 hr F	-	-	
38	95.33	119.81	.759	98.0	.774	.436	100	7.4	29	60.0 hr F	-	-	
45	95.18	119.88	.767	98.7	.777	.437	100	7.4	29	60.1 hr F	-	-	
48	95.98	120.43	.753	98.8	.762	.432	100	7.4	29	60.0 hr F	-	-	
<u>Average instantaneous strength = 1340 psi</u>													
<u>Nominal temp 31°F</u>													
8	95.07	119.71	.766	98.7	.779	.438	775	96.3	31	76.3"	-	-	0.101
9	94.99	119.61	.766	98.1	.780	.438	853	106.0	31	16.9"	-	-	0.0397
10	95.47	120.00	.759	98.4	.771	.435	734	91.2	31	9.8"	-	-	0.140
15	94.73	119.53	.774	98.5	.785	.440	833	103.5	31	19.8"	-	-	0.0401
18	96.56	119.75	.710	94.4	.751	.429	828	102.9	31	-	-	-	L.M.P. holder loose
20	95.32	119.88	.761	98.3	.774	.436	808	100.4	31	57.9"	-	-	0.0925
21 V	95.22	119.97	.768	99.3	.776	.457	280	34.8	31	5.5 hr	3.0	0.175	
41 V	94.45	119.42	.781	98.8	.790	.441	280	34.8	31	5.5 hr	3.0	0.185	
37 V	93.92	119.15	.793	98.7	.803	.446	160	19.9	31	80 hr	48.0	0.27	
42 V	94.0	119.13	.790	98.8	.799	.444	160	19.9	31	80 hr	58.0	0.20	
13 V	95.27	119.79	.761	98.1	.775	.437	150	18.6	31	24 hr F	-	-	Weight on STOPS
14 V	94.91	119.65	.770	98.5	.781	.439	150	18.6	31	104 hr F	57.0	0.17	
16 V	94.88	119.63	.771	98.5	.782	.439	150	18.6	31	144 hr F	80.0	0.16	
5 V	94.83	119.71	.775	99.0	.783	.439	80	9.9	31	149 hr F	-	-	Weight on STOPS
17 V	94.83	119.55	.775	98.9	.783	.439	80	9.9	31	139.7 hr	-	-	
12	94.76	119.64	.776	98.9	.785	.440	20	2.5	31	257 hr	-	-	
24	95.31	119.90	.762	98.4	.774	.436	20	2.5	31	864 hr F	-	-	
<u>Average instantaneous strength = 805 psi</u>													
y_d	Dry unit wt	y_m	Void ratio	$\frac{V_1}{V_S}$	Mass unit wt	$P.F.$	ϵ	Point of time-strain curve where plastic flow begins					
y_m	Mass unit wt	V_1	Max. stress	$\frac{S_1}{V_S}$	Vol. of ice	$P.F.*$	*	Duration of test					
			Vol. of soil grains	S_1	Vol. of voids filled with ice	F		Tests performed on constant stress apparatus					

y_d = Dry unit wt
 y_m = Mass unit wt
 $\frac{V_1}{V_S}$ = Vol. of ice
 $\frac{S_1}{V_S}$ = Vol. of soil grains
 S_1 = Percent of voids filled with ice
 $P.F.$ = Point of time-strain curve where plastic flow begins
 $P.F.*$ = Max. stress
 F = Duration of test
 V = Tests performed on constant stress apparatus
 ϵ = Void ratio
 ϵ = Point of time-strain curve where plastic flow begins
 ϵ = Point of time-strain curve where plastic flow begins

APPENDIX A

Table AIII. Ice.

Specimen No.	Stress lb/in. ² g/cm ³	% of Inst. Strength (initial)	Temp °F	Time to fail	Failure strain	Remarks
<u>Nominal temp 25F</u>						
ICE-10	0.914	481*	98.2	25	4.2"	- LMP failure
ICE-12	0.914	478*	97.6	25	4.0"	.0000756
ICE-22	0.912	510*	104.1	25	4.2"	- LMP failure
ICE-11	0.915	170	34.7	25	49 hr F†	- Specimen tilted
ICE- 9	0.914	100	20.4	25	408 hr F†	-
ICE-14	0.915	50	10.2	25	791 hr F†	-

Average instantaneous strength = 490 psi

<u>Nominal temp 29F</u>						
ICE- 6	0.903	259*	96.3	29	1.8"	.0000585
ICE-20	0.915	263*	97.8	29	2.1"	.000498
ICE-21	0.914	285*	105.9	29	2.3"	.001281
ICE-16	0.914	160	59.5	29	2.5 hr F†	-
ICE-15	0.913	95	35.3	29	627 hr F†	-
ICE- 2	0.914	54	20.1	29	863 hr F†	-
ICE- 8	0.912	27	10.0	29	1055 hr F†	-

Average instantaneous strength = 269 psi

* Max. stress

† Duration of test

Unclassified

Security Classification

DOCUMENT CONTROL DATA - R & D

(Security classification of title, body of abstract and indexing annotation must be entered when the overall report is classified)

1. ORIGINATING ACTIVITY (Corporate author) Cold Regions Research and Engineering Laboratory U.S. Army Terrestrial Sciences Center, Hanover, New Hampshire	2a. REPORT SECURITY CLASSIFICATION Unclassified
	2b. GROUP

2. REPORT TITLE

CREEP OF FROZEN SANDS

4. DESCRIPTIVE NOTES (Type of report and inclusive dates)

Technical Report

5. AUTHOR(S) (First name, middle initial, last name)

Francis H. Sayles

6. REPORT DATE September 1968	7a. TOTAL NO. OF PAGES 60	7b. NO. OF REFS 13
8a. CONTRACT OR GRANT NO.	9a. ORIGINATOR'S REPORT NUMBER(S)	
8b. PROJECT NO.	Technical Report 190	
c.	9b. OTHER REPORT NO(S) (Any other numbers that may be assigned to this report)	
d.		

10. DISTRIBUTION STATEMENT

This document has been approved for public release and sale; its distribution is unlimited.

11. SUPPLEMENTARY NOTES	12. SPONSORING MILITARY ACTIVITY Office, Chief of Engineers Directorate of Military Construction Engineering Division Civil Engineering Branch
-------------------------	--

13. ABSTRACT

Unconfined compressive creep strengths and strains were measured for frozen saturated Ottawa sand (20-30) and Manchester fine sand. The creep tests were conducted at approximate stress levels of 60, 35, 20 and 5% of the conventional unconfined compressive strength. Testing temperatures were 15, 25, 29 and 31F. It was found that the unconfined compressive creep strength of the frozen sand can be predicted using two short-term, high-stress-level creep tests. using $\epsilon = \epsilon_1 + (t^{\psi}/\psi)$; that total strain can be predicted using $\epsilon = \left[\frac{\sigma}{\sigma_{01} \theta_0^{\alpha} (\theta/\theta_0) + 1} \right]^{\alpha} \frac{t^{\psi}}{\psi} + \epsilon_0$; and that for stresses below the long-term strength, the strain rate is directly proportional to the reciprocal of time during stress action until complete stabilization occurs. (ϵ_1 = strain rate 1 hour after stress is applied; t = time; $\psi = (M-1)/M$, where $M = \sigma^{1/w}$ and w is a constant for each material; θ_0 = stress at $\theta = 0$; θ = temperature in degrees below freezing point of water; θ_0 = a constant reference value of θ ; α and K are constants; ϵ_0 = initial instantaneous strain.)

Unclassified

Security Classification

14. KEY WORDS	LINK A		LINK B		LINK C	
	ROLE	WT	ROLE	WT	ROLE	WT
Soils Sand Permafrost Frozen soil - strength - creep - stress - deformation						

Unclassified

Security Classification